Bioactive Materials 19 (2023) 550–568

Contents lists available at ScienceDirect

Bioactive Materials

journal homepage: www.keaipublishing.com/en/journals/bioactive-materials

# A reactive oxygen species-responsive hydrogel encapsulated with bone marrow derived stem cells promotes repair and regeneration of spinal cord injury

Ziming Li [a,1], Tengfei Zhao [b,1], Jie Ding [a], Haochen Gu [c], Qiaoxuan Wang [a], Yifan Wang [b], Deteng Zhang [a,d,**], Changyou Gao [a,e,*]

[a] MOE Key Laboratory of Macromolecular Synthesis and Functionalization, Department of Polymer Science and Engineering, Zhejiang University, Hangzhou 310027, China
[b] Department of Orthopedics, the Second Affiliated Hospital of Zhejiang University, Hangzhou 310009, China
[c] School of Medicine, Zhejiang University, Hangzhou 310009, China
[d] Institute of Neuroregeneration and Neurorehabilitation, Qingdao University, Qingdao 266071, China
[e] Dr. Li Dak Sum & Yip Yio Chin Center for Stem Cell and Regenerative Medicine, Zhejiang University, Hangzhou 310058, China

ARTICLE INFO

*Keywords:*
Spinal cord injury (SCI)
ROS scavenging
BMSCs
Axon regeneration
Anti-oxidation

ABSTRACT

Spinal cord injury (SCI) is an overwhelming and incurable disabling event accompanied by complicated inflammation-related pathological processes, such as excessive reactive oxygen species (ROS) produced by the infiltrated inflammatory immune cells and released to the extracellular microenvironment, leading to the widespread apoptosis of the neuron cells, glial and oligodendroctyes. In this study, a thioketal-containing and ROS-scavenging hydrogel was prepared for encapsulation of the bone marrow derived mesenchymal stem cells (BMSCs), which promoted the neurogenesis and axon regeneration by scavenging the overproduced ROS and rebuilding a regenerative microenvironment. The hydrogel could effectively encapsulate BMSCs, and played a remarkable neuroprotective role *in vivo* by reducing the production of endogenous ROS, attenuating ROS-mediated oxidative damage and downregulating the inflammatory cytokines such as interleukin-1 beta (IL-1β), interleukin-6 (IL-6) and tumor necrosis factor-alpha (TNF-α), resulting in a reduced cell apoptosis in the spinal cord tissue. The BMSCs-encapsulated ROS-scavenging hydrogel also reduced the scar formation, and improved the neurogenesis of the spinal cord tissue, and thus distinctly enhanced the motor functional recovery of SCI rats. Our work provides a combinational strategy against ROS-mediated oxidative stress, with potential applications not only in SCI, but also in other central nervous system diseases with similar pathological conditions.

## 1. Introduction

As a catastrophic event, traumatic spinal cord injury (SCI) can cause an impairment or dysfunction in locomotor and sensory, bringing life-changing paralysis, severe complications and even death to patients [1,2]. Up to now, there have been 27 million global SCI cases with 93.8 thousand new occurrence each year [3]. Nonetheless, the current clinical therapies for SCI cannot achieve satisfactory efficacy of axon regeneration, not to mention the effective motor restoration [4,5].

After trauma-caused primary injuries, numerous severe complications of secondary injuries occur surrounding the lesion site, including uncontrolled oxidative stress and inflammation, tissue remodeling, cytotoxic neural excitement caused by rapid and vast influx of calcium ions and glutamate, resulting in the necrosis and apoptosis of neurons

Peer review under responsibility of KeAi Communications Co., Ltd.
* Corresponding author. MOE Key Laboratory of Macromolecular Synthesis and Functionalization, Department of Polymer Science and Engineering, Zhejiang University, Hangzhou, 310027, China.
** Corresponding author. MOE Key Laboratory of Macromolecular Synthesis and Functionalization, Department of Polymer Science and Engineering, Zhejiang University, Hangzhou, 310027, China.
*E-mail addresses:* zhangbio137@qdu.edu.cn (D. Zhang), cygao@zju.edu.cn (C. Gao).
[1] These authors contributed equally to this work.

https://doi.org/10.1016/j.bioactmat.2022.04.029
Received 3 February 2022; Received in revised form 13 April 2022; Accepted 22 April 2022

and glial cells that together contribute to the neuron loss [6,7]. So far, a majority of the treatment for SCI lie in the application of biocompatible polymers to reduce secondary inflammation [8,9], the design of patterned hydrogels or oriented scaffolds to guide the regenerated axons [10,11], immune cells polarization-regulating nanoparticles or hydrogels [12,13], and the cell transplantation [14,15]. For instance, a polycaprolactone (PCL) nanofiber-modified hydrogel consisting of hyaluronic acid (HA) and poly(ethylene glycol) diacrylate (PEGDA) promotes macrophage polarization in a rat SCI model, leading to the enhanced immature neuron amount and axon density [16]. Other types of scaffolds such as an imidazole-conjugated poly(organophosphazenes) hydrogel for macrophage-targeting [17] and chitosan micro-hydrogels [18] are also used for SCI therapy. However, without the specific addition or encapsulation of the neurogenesis-promoting biomolecules or stem cells, the efficacy on motor recovery after treatment with these biomaterials remains insufficient. On the other hand, although the damaged neurons can be replaced with stem cells such as mesenchymal stem cells (MSCs), low bioavailability in the lesion site and insufficient behavior restoration efficacy towards severe paraplegia cases still limit their application.

Nonetheless, transplantation of stem cells with hydrogels is a promising therapy for SCI, in which the hydrogels provide an artificial extracellular matrix (ECM) for the implanted cells, act as a physical barrier to avoid the unexpected and unfavorable diffusion, and attenuate the secondary inflammation induced by mechanical mismatch [19,20]. Nonetheless, the therapeutic effect by using non-stimuli responsive hydrogels is inadequate because most of the implanted cells may not survive in the cytotoxic and inhibitory microenvironment [21].

The overproduced reactive oxygen species (ROS) are regarded as one of the chief culprits because they induce oxidative stress, cytotoxic neuro-excitement and a new round of severe inflammatory response [22,23]. It was reported that the coenzyme Q10 can regulate the apoptosis and oxidative stress, and protect the transplanted BMSCs to improve their therapeutic efficiency for SCI [24]. Nonetheless, its comparative slow adsorption and chemically unstable nature may lead to low bioavailability and thus a comparative low protection *in vivo* [25,26].

The scavenging of overproduced ROS with biomaterials can successfully regulate the hostile environment, protect transplanted cells and significantly promote neurogenesis. Kim et al. [27] injected an optimal dose of cerium oxide nanoparticles (CONPs) to the lesion site, resulting in a reduced cavity size and inflammatory cells, accompanied with downregulated mRNA expression of inflammatory cytokines and apoptotic proteins. Similarly, selenium nanoparticles (Se NPs) [28], iron oxide NPs [29], Mn (III) tetrakis (4-benzoic acid) porphyrin NPs [30] can also minimize the ROS in SCI treatment. Besides, the polymer-based ROS scavenging biomaterials are also efficient in SCI treatment, and have their unique advantages such as adjustable degradability and harmless degradable products. So far, tetramethylpiperidine 1-oxyl (Tempol)-grafted hydrogel [31] and high-density thioether-containing lipid-polymer nanoparticles [32] have been successfully reported for ROS-scavenging in SCI. Li et al. [21] transplanted a $MnO_2$ nanoparticles ($MnO_2$ NPs)-dotted HA hydrogel with bone-derived MSCs (BMSCs), and proved that the $MnO_2$ NPs significantly protect the BMSCs against ROS-abundant microenvironment, while the BMSCs encapsulated in the undotted hydrogel sustain a great loss. However, little attention has been paid to the combination of stem cells and ROS-scavenging hydrogels for SCI treatment, which has the comprehensive advantages in modulating the inflammatory microenvironment and protecting the encapsulated stem cells against apoptosis, resulting in a better SCI therapy *in vivo*.

In this study, a thioketal-containing hyperbranched polymer (HBPAK) is crosslinked with methacrylate hyaluronic acid (HA-MA) to form a ROS-responsive and scavenging hydrogel, in which neural specific CQAASIKVAV peptides (IKVAV in short) are covalently grafted and rat-derived epidermal growth factor (EGF) and rat-derived basic fibroblast growth factor (bFGF) are physically encapsulated. This hydrogel is able to scavenge overproduced ROS, promote the polarization of M2 macrophages, alleviate the inflammation, and protect the encapsulated BMSCs against oxidative stress when transplantation for SCI treatment *in vivo* (Scheme 1). The fundamental physiochemical properties of the obtained hydrogel and its anti-oxidation, anti-inflammation and biocompatibility are characterized *in vitro*. A rat transection spinal cord injury model at the $10^{th}$ thoracic (T10) level (2 mm) is used to assay the *in vivo* therapeutic effect, especially the anti-oxidation and axon regeneration.

## 2. Materials and methods

### 2.1. Materials

Hyaluronic acid (HA, Mw = 100 kDa, Haihua, Jiangsu, China), methacrylic anhydride (MA, Sigma-Aldrich, USA), cysteine hydrochloride (Aladdin, Shanghai, China), poly(ethylene glycol) diacrylate with a molecular weight of 575 ($PEGDA_{575}$, Sigma-Aldrich, USA), thiol-containing IKVAV peptide (CQAASIKVAV, GL Biochem., Shanghai, China), EGF (PeproTech, USA) and bFGF (PeproTech, USA) were used as received without further purification. *N*,*N*-Dimethylformamide (DMF), dimethyl sulfoxide (DMSO), and methyl *tert*-butyl ether were all purchased from China National Pharmaceutical Group Corporation. The Live/Dead staining kit was obtained from Beyotime Biotechnology (Shanghai, China). The inhibition and production superoxide anion assay kit was purchased from Nanjing Jiancheng Bioengineering Institute (Nanjing, China). The antibodies of anti-α-smooth muscle actin (α-SMA), anti-CD31, anti-CD86, anti-CD163, anti-MAP2 and anti-8-hydroxy-2 deoxyguanosine (anti-8-OHdG) were all purchased from Abcam (Shanghai, China). Cell Counting Kit-8 (CCK-8) was purchased from 7Sea Biotech Co. Ltd (Shanghai, China). The antibodies of anti-neurofilament 200 (anti-NF200), anti-class III beta tubulin (anti-Tuj-1) and anti-platelet derived growth factor subunit-β (anti-PDGFR-β) were all purchased from Cell Signaling Technology (CST, Boston, USA). Rat tumor necrosis factor-α (TNF-α), interleukin-1β (IL-1β) and IL-6 enzyme-linked immunosorbent assay (ELISA) Research Reagent and anti-glial fibrillary acidic protein (anti-GFAP) were purchased from Boster (Wuhan, China). Dihydroethidium (DHE) kit was purchased from Yeason (Shanghai, China). Alpha-minimum essential medium (α-MEM), high glucose Dulbecco's modified Eagle medium (DMEM), fetal bovine serum (FBS) and anti-biotic mixture containing penicillin and penicillin were all purchased from Gibco (New York, USA). Ultra-purified water used in this study was prepared by Milli-Q cycle purification system (Millipore, USA).

### 2.2. Synthesis and characterization of HBPAK and HA-MA

The ROS-responsive hyperbranched polymers (HBPAK) were synthesized through a Michael addition reaction between the PEGDA with end-capped double bonds and ROS-cleavable thioketal diamine (TK) according to a method reported previously [33]. To confirm the structures of TK and HBPAK, 10 mg TK and HBPAK were fully dissolved in deuterated chloroform ($CDCl_3$) or deuterated dimethyl sulfoxide ($DMSO\text{-}D_6$), respectively, and were characterized using 500 MHz $^1H$ nuclear magnetic resonance ($^1H$ NMR). The weight-average molecular weight (Mw) and polydispersity (PDI) was measured by hydrogel permeation chromatography (GPC, Waters 1515) after the HBPAK was dissolved in *N*,*N*-dimethylformamide (DMF) to reach a concentration of 5 mg/mL. The ROS-scavenging abilities were confirmed by assays using hydrogen peroxide ($H_2O_2$) and 1′-diphenyl-2-picrylhydrazyl (DPPH) according to the previously reported methods [34,35].

Methacrylate hyaluronic acid (HA-MA) was synthesized by referring to a previously reported method [33] with minor modification. Briefly, 2 g HA was completely dissolved in a solution containing 66.7 mL DMF and 133.3 mL water overnight, into which 15 mL MA was added drop by drop in an ice bath with addition of a proper volume of 5 M NaOH to

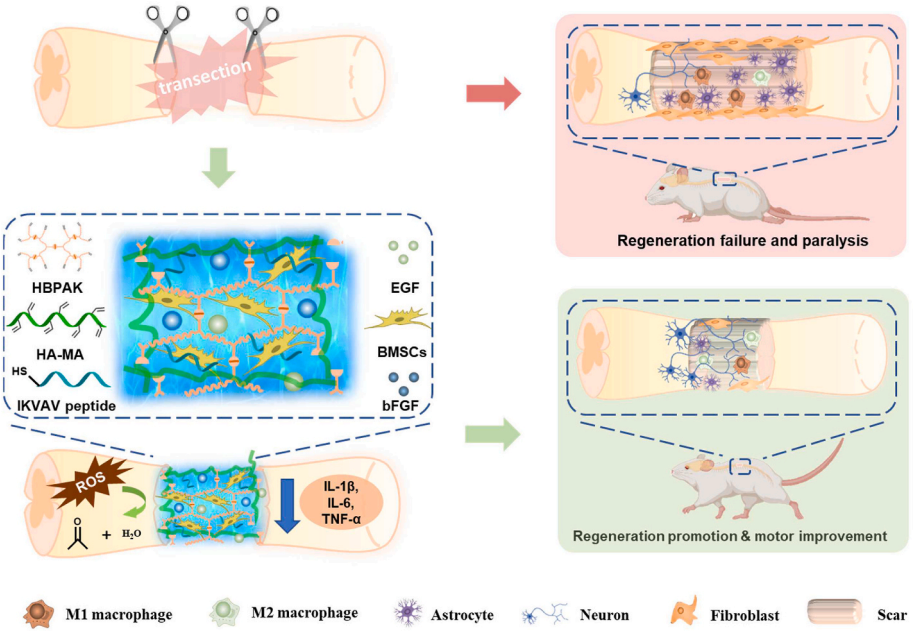


**Scheme 1.** Schematic illustration of the BMSCs-encapsulated ROS-scavenging hydrogel for spinal cord injury treatment. After SCI, the BMSCs-encapsulated ROS-scavenging hydrogel (THIEF-Cell) can eliminate the over-produced ROS to achieve better neuron proration, and significantly improve neurogenesis and motor recovery while attenuate scar formation.

maintain the pH 8–9. After 12 h, the product was precipitated by ethanol with 9 times volume of the HA solution, and collected by centrifugation at 8000 rpm for 5 min. The precipitate was re-dissolved in water, and dialyzed for 5 days before lyophilization. The HA-MA was fully dissolved in $D_2O$ with a concentration of 10 mg/mL for $^1H$ NMR characterization, according to which the grafting ratio of MA was calculated as described in SI [33].

### 2.3. Preparation and characterization of hydrogels

#### 2.3.1. Gelation of hydrogels

HBPAK, HA-MA, IKVAV and lithium phenyl-2,4,6-trimethylbenzoylphosphinate (LAP) were dissolved in phosphate buffered saline (PBS) in sequence in dark to achieve a final mixture prepolymer solution consisting of 1% w/v HA-MA, 10% w/v HBPAK, 500 μg/mL IKVAV peptides and 0.5‰ w/v LAP. This mixture solution could be gelated in 30 s under the 365 nm UV light irradiation in a UV-light curing oven (LAMP Technology) with a power of 50 mW/cm$^2$ to obtain the thioketal- and HA-containing ROS-scavenging hydrogel with IKVAV peptide modification (THI hydrogel). Other hydrogels with different compositions were obtained in the same way. The thioketal- and HA-containing ROS-scavenging hydrogel without IKVAV peptide modification was denoted as TH hydrogel. Similarly, the ROS-scavenging hydrogel with IKVAV peptide modification and loading of EGF and bFGF was denoted as the THIEF hydrogel. To obtain the THIEF hydrogel, the EGF solution and bFGF solution were added into the prepolymer solution with a final concentration of EGF and bFGF up to 21 μg/mL, respectively. Moreover, keeping the other components same, the HBPAK was replaced by the non-ROS responsive PEGDA575 to prepare the non-ROS scavenging hydrogels, which were denoted as the PH hydrogel, PHI hydrogel and PHIEF hydrogel, according to the presence or absence of IKVAV peptide and/or growth factors in the hydrogels. Specially, the prepolymer solutions of different hydrogels for *in vitro* cell and *in vivo* animal experiments were filtrated twice with 0.22 μm hydrophilic membranes to remove bacteria. For animal experiment, about 30 μL pre-hydrogel solution was gelated in a mold to form a column (2.5 mm × 2.0 mm × 2.5 mm).

#### 2.3.2. Compression test

The hydrogels in a column shape (φ = 8 mm, h = 5.5 mm) were characterized by using a universal mechanical testing instrument (5543A, Instron, USA) with a compression rate of 0.2 mm/min. The compressive modulus was calculated according to the slope of the initial linear part of the stress–strain curves.

#### 2.3.3. Rheological test

Different hydrogels were characterized by using a rotational rheometer (HAAKE, RS6000) with a rotator diameter of 20 mm. The strain-sweep tests were conducted at 37 °C and 6.28 rad/s to confirm that a 1% strain was in the linear viscoelastic region. The frequency-sweep tests were then carried out from 0.1 rad/s to 100 rad/s to show the mechanical changes of storage modulus ($G'$) and loss modulus ($G''$) of the hydrogels at different rotation frequency, where the temperature was kept at 37 °C and the strain was maintained at 1%. The time-sweep tests were conducted at a temperature of 37 °C, a rotate frequency of 6.28 rad/s and a strain of 1% to reveal a long-time mechanical stability and meanwhile, to calculate an average $G'$ and $G''$ of each type of hydrogels.

#### 2.3.4. Characterization of IKVAV binding to the hydrogel

For characterization of IKVAV binding to the hydrogel, 500 μL THI hydrogel and PHI hydrogel (containing 250 μg IKVAV peptides) were prepared, which were then incubated in 500 μL PBS overnight, respectively. High performance liquid chromatography (HPLC, Waters 1525, USA) was used to detect the IKVAV peptide amount in the extracts. As a control, a series of pure IKVAV peptide solutions with concentrations of 15.6, 31.25, 62.5, 125, 250 and 500 μg/mL were detected by HPLC to construct a calibration curve. Moreover, 5,5′-dithiobis-(2-nitrobenzoic acid) (DTNB, also known as Ellman's reagent) assay was used to substantiate the IKVAV binding by referring to a method reported previously [36]. In brief, 250 μL hydrogel of each group was prepared and immersed into PBS overnight to obtain the extracts, which were reacted with DTNB solution overnight before the optical density (OD) value was detected by a microplate reader (TECAN INFINITE M200PRO). The OD values of a series of pure IKVAV peptide solutions were measured and used as a control.

#### 2.3.5. Degradation

For hydrolysis and ROS-responsive degradation detection, two different hydrogels (THI hydrogel and PHI hydrogel) were soaked into PBS overnight in advance for swelling equilibrium, weighed by an electronic balance ($m_0$). The hydrogels were then immersed in PBS or PBS containing 200 μM $H_2O_2$ at 37 °C, respectively. The wet weight of hydrogels ($m_w$) was recorded at different time, and the solutions were replaced by new ones every day, respectively. The weight remaining was calculated as $m_w/m_0 \times 100\%$.

#### 2.3.6. DPPH scavenging

The DPPH scavenging capacity of different hydrogels (TH gel, THI gel, PH gel and PHI gel) was assessed by incubating 200 μL hydrogel in 200 μM DPPH ethanol solution in dark. The absorbance of the immersed solution or pure DPPH ethanol solution was detected at 517 nm. The ability of DPPH radical scavenging was calculated as described in SI.

#### 2.3.7. $H_2O_2$ scavenging

After the $H_2O_2$ scavenging capacity of THI hydrogel and PHI hydrogel was assayed by incubating 200 μL hydrogel in 1 mL 100 μM $H_2O_2$ solution for 0.5 h at 37 °C in dark, 1 mL 1 M KI solution was added. 5 min later, 1 mL of the final solution was drawn to test the absorbance curves by UV–vis spectroscopy.

#### 2.3.8. $O_2^-$ scavenging

The·$O_2^-$ scavenging capacity was testified by using 200 μL TH hydrogel, THI hydrogel, PH hydrogel and PHI hydrogel according to the instruction of the inhibition and production superoxide anion assay kit (Nanjing Jiancheng Bioengineering Institute, China). After reaction for 5 min, 1 mL of the final solution was tested for the absorbance curves *via* UV–vis spectroscopy, and 400 μL final solution was used for OD value detection at 550 nm ($OD_{sample}$). The OD value of the reagents reacted with equivalent volume of water was set as a control ($OD_{control}$), and that of pure water was set as blank ($OD_{water}$). The scavenging ratio was calculated as $(OD_{sample} - OD_{water})/(OD_{control} - OD_{water}) \times 100\%$

### 2.4. Cell experiments

#### 2.4.1. Isolation and Subculture of BMSCs

BMSCs were harvested from the tibias of Sprague-Dawley rats (SD rats, 6–8 weeks, about 120 g, male, total 20 donor rats) and cultured in α-MEM according to a previously reported method [37]. The BMSCs were incubated at 37 °C in 5% $CO_2$ atmosphere within a humidified cell incubator. Unless noted otherwise, the mediums used in this study (α-MEM and high glucose DMEM included) were all added with 10% v/v FBS, 100 U/mL penicillin and 100 μg/mL streptomycin. The cells at passage 3 to 5 were used for all experiments.

#### 2.4.2. Resuscitation and Subculture of Schwann cells

For resuscitation, SD rat Schwann cells from liquid nitrogen were immediately immersed into water at 37 °C to melt and then, resuspended with high glucose DMEM. Afterwards, the cell suspension was centrifuged to remove DMSO and re-cultured by referring to a method reported previously [38].

#### 2.4.3. Resuscitation and Subculture of Raw 264.7

Mouse-derived Raw 264.7 cells were resuscitated and sub-cultured similar to the Schwann cells except that the period of passage cultivation was less than 2 days and the passage ratio was 1:5.

#### 2.4.4. Cytotoxicity assay of different hydrogels in vitro

Different types of hydrogels (TH hydrogel, THI hydrogel, PH hydrogel and PHI hydrogel) were fully immersed in mediums at a concentration of 50 mg/mL for 24 h at 37 °C. The Schwann cells or BMSCs with a density of 5000 cells/well were incubated with the responding medium in a 96-well tissue culture plate (TCPS) for 24 h, before the cell adhesion to the culture plate was measured. The cells were cultured and incubated with hydrogel extracts for another 24 h. After the culture medium was removed, the cells were washed three times with excessive PBS, and then replaced by a new medium containing 10% v/v CCK-8. These samples were maintained in dark for 2 h in a cell incubator. The OD values of cells being co-incubated with hydrogel extracts ($OD_{sample}$) or with medium merely ($OD_{control}$) were compared with that of the pure CCK-8 solution ($OD_{cck\text{-}8}$) at 450 nm. The OD values of CCK-8 being co-incubated with extracts without cells were also tested to exclude the possibility that the redox substance in extracts may interfere the CCK-8 chromogenic reaction. The cell viability was calculated as

$$\text{cell viability } (\%) = \frac{OD_{sample} - OD_{cck-8}}{OD_{control} - OD_{cck-8}} \times 100\%$$

Similarly, to evaluate the cytotoxicity of the degradation products towards BMSCs, different hydrogels were immersed in medium and incubated for 3 days or 7 days to allow the degradation. Afterwards, the CCK-8 assay was performed.

#### 2.4.5. Live/Dead staining of BMSCs being encapsulated in hydrogel in vitro

BMSCs were harvested when their attachment rate reached 70~80%, and resuspended in the as-prepared prepolymer solutions of hydrogels with a density of $8 \times 10^6$ cell/mL. Then, 200 μL cell-suspending prepolymer solutions were gelated within 30 s to form different BMSC-encapsulated hydrogel groups under UV-irradiation. Subsequently, the hydrogels were transferred to 24-well TCPS, into which 800 μL α-MEM medium was added to each well. The cells in the hydrogels were cultured for 1, 3 or 7 days with medium changing every day. Before Live/Dead staining, the medium was removed, and each well was washed with excessive PBS for several times. Calcein AM for live staining and propidium iodide (PI) for dead staining were diluted 500 times each by buffer in kit, and then co-incubated with the cells in dark at 37 °C in an incubator. After 10 min incubation, the staining dye was removed, and the hydrogels with cells were washed with excessive PBS triple times, each for 5 min. Finally, the fluorescent images were taken by a fluorescence microscope (Olympus, IX81, Japan), which were quantified by Image J Software to compare the cell number and viability changes.

#### 2.4.6. Simulated inflammatory micro-environment in vitro

A simulated inflammatory environment *in vitro* was created by using Transwell chamber to explore the protection of encapsulated BMSCs against oxidative damage in the inflammation process of SCI. Generally, for simulated inflammation-mediated activation, Raw 264.7 cells at a density of 200,000 per well were planted on a 6-well TCPs-, and cultured overnight to allow cell adhesion. The normal medium was then replaced with a serum-free medium supplemented with lipopolysaccharide (LPS) and interferon-γ (IFN-γ) with final concentrations of 1 μg/mL and 200 ng/mL, respectively, which stimulated the Raw 264.7 cells towards an inflammatory phenotype for 12 h. The BMSCs-encapsulated hydrogels (300 μL) with a final cell density of $8 \times 10^6$/mL (THIEF-Cell and PHIEF-Cell) were placed on the upper Transwell chamber before 1 mL serum-free α-MEM medium was added. Here, the serum-free medium was used because that the serum may combine with LPS and IFN-γ, weakening the stimulation efficacy. The Live/Dead staining assay was conducted to characterize their cytoviability after culture for 1 day.

The modulation of inflammatory macrophages was further characterized after they were induced by LBS/INF-γ. In brief, 300 μL THIEF hydrogel and PHIEF hydrogel, and THIEF-Cell and PHIEF-Cell with a cell density of $8 \times 10^6$/mL were placed on the upper Transwell chamber and cultured in 1 mL α-MEM medium. Moreover, BMSCs with the same quantity were planted on the upper Transwell chamber (2D BMSCs group) as a control. The stimulated macrophages without any cell or material treatment, and the non-stimulated macrophages were set as the control groups too. DCFH-DA, a ROS fluorescent probe, was used to label the macrophages collected at the lower Transwell chamber after 1 day

culture. The DCF fluorescence intensity of the DCFH-DA stained macrophages was analyzed by flow cytometry (BD FACS Calibur with CellQuest software, BD Biosciences, USA). Finally, the culture mediums of Raw 264.7 cells in each group were collected for detection of the secreted pro-inflammatory IL-6 and TNF-α cytokines by ELISA assay [39].

The transcription levels of CD86, IL-6 and TNF-α were investigated. The total RNAs of macrophages collected at the lower Transwell chamber from each group after 1 day culture were extracted by using the Trizol reagent according to the manual. 1 μg of RNA was converted to complementary DNA (cDNA) by the All-in-One First-Strand cDNA Synthesis SuperMix for qPCR (TRAN) after the concentration of RNA was measured by a NanoDrop 2000 spectrophotometer (Thermo, USA). Then, qRT-PCR was performed in triplicate with 2X SYBR Green qPCR Master Mix (APExBIO) for the quantitative analysis of target gene expression. The expression level of each gene was normalized to the house-keeping gene (18s RNA). The primer sequences are listed in Table S1.

### 2.5. In vivo experiments

#### 2.5.1. Surgery for spinal cord transection and hydrogel implantation

The SD rats (8 weeks, 200–250 g, female) were purchased from Zhejiang Academy of Medical Sciences, China. The animal experiment operations were approved by the Experimental Animal Ethics Committee of Hangzhou Medical College (Application Number: 200020015). Before surgery, the SD rats were withholding for foods and liquids for 1 day to prevent gastrointestinal flatulence and excessive respiratory secretions in animals. The operating room was fully sterilized by UV irradiation for 30 min. After weighing and anesthesia for half an hour with 1% v/v sodium pentobarbital (4.5 mL/kg) via intraperitoneal injection, the hair next to the T10 spine on the back of the SD rats was shaved, and the operative region was completely sterilized with iodophor. The skin was cut along the midline of the back, and the surrounding muscles were separated and the vertebral plate was detached to expose the dorsal of T9–10 segment. The spinal cord was transected to form a $2.0 \pm 0.5$ mm gap with the complete transection of the meninges. After complete hemostasis, the THI hydrogel, THIEF-Cells and PHIEF-Cells were implanted into the gap of the lesion site, respectively. The SCI group without any treatment was set as the control. Ultimately, the muscle and skin were well sutured. For surgical care, 2.0 mL saline was intraperitoneally injected pre-surgery, during surgery and post-surgery, respectively. $2 \times 10^5$ U penicillin per day was provided via intraperitoneal injection to prevent urinary tract infection for 2 weeks after surgery, and the rats got bladder massage twice every day for nearly a month for manual auxiliary urination. Comprehensively, 75 rats were used in these *in vivo* studies and 15 died during the surgery or feeding. Totally 60 survived at the end of this study for the THIEF-Cell (19), THI gel (14), PHIEF-Cell (15) and SCI (12) groups.

#### 2.5.2. Locomotor function investigation

Recovery of rat hind limb motor functions was evaluated weekly post-surgery according to the 21-point Basso-Beattie-Bresnahan locomotor rating scale (BBB scale). Different groups of rats were allowed to walk freely in an open field. Two independent observers who were blinded to the groups of experiment evaluated the motor behavior within 3 min for rats. Results were analyzed through OriginLab Pro 2021.

#### 2.5.3. Tissue processing

The rats were painlessly sacrificed by intraperitoneal injection of 4% v/v chloral hydrate at day 7 post-surgery for evaluation of anti-oxidation and anti-inflammation properties, and at day 56 post-surgery for evaluating the axon regeneration and vascularization. For tissue immunohistochemistry and immunofluorescence evaluation, the rats were perfused with excessive isotonic physiological saline and then replaced by 4% v/v paraformaldehyde (PFA). Afterwards, the spinal cords were separated with a total length of 1.5 cm containing the lesion site at the middle, which were immersed in 4% PFA v/v for 48 h at 4 °C for further fixation and processing. To detect the pro-inflammatory cytokines by ELISA, the spinal cord tissues were directly harvested under deep anesthesia and transferred to liquid nitrogen immediately.

#### 2.5.4. Immunohistochemistry and immunofluorescence

After removal of formaldehyde and dehydration, the as-fixed spinal cord tissues were embedded in paraffin and sectioned into 10 μm slices for staining. Hematoxylin & eosin (H&E), Masson, Nissl and terminal-deoxynucleoitidyl transferase dediated nick end labeling (TUNEL) staining was performed according to the standard procedures. After 4 °C acetone fixation, the sections were co-incubated with solutions of different primary antibodies with a dilution ratio of 1:400, including anti-8-OHdG, anti-CD86, anti-CD163, anti-PDGFR-β, anti-GFAP, anti-NF200, anti-Tuj-1, and anti-MAP-2 at 4 °C overnight. Fluorescein isothiocynate (FITC) and/or phycoerythrin (PE)-conjugated secondary antibodies were diluted with a ratio of 1:400 and then were used to incubate with the sections at 37 °C for 1 h. 4′,6-Diamidino-2-phenylindole dihydrochloride (DAPI, Sigma, St. Louis, USA) was used for nuclei labeling. The samples were observed using laser scanning confocal microscopy (LSM710NLO, Zeiss, Germany) with identical exposure time. The lesion site (2 mm), as well as the rostral and the caudal site (each was 0.5 mm next to the lesion site) were selected and imaged as the investigated region of interest (ROI) per section.

#### 2.5.5. ELISA assay

The collected spinal cord tissues were transferred into centrifuge tubes, into which moderate PBS was added. The tissues were disrupted by an ultrasonic homogenizer to obtain milky white suspensions, which were centrifugated at 12,000 rpm for 10 min to harvest the supernatants, respectively. The IL-1β, IL-6 and TNF-α were determined by corresponding ELISA kits following the manual instruction.

### 2.6. Statistical analysis

The quantitative data were shown by mean ± standard deviation (SD). Statistical analysis among groups is conducted by ANOVA and *t*-test with OriginLab Pro 2021. The significant difference is expressed as $^*p < 0.05$, $^{**}p < 0.01$ and $^{***}p < 0.001$, respectively. The n quals to 4 if not specially stated.

## 3. Results and discussion

### 3.1. Preparation and characterization of hydrogels

Biocompatible natural polymers such as HA, gelatin, chitosan and collagen are conducive to and widely used in axon regeneration. Most of the natural polymer-based hydrogels have a matched mechanical modulus to the natural spinal cord tissue, preventing secondary injuries caused by mismatched mechanical properties, and minimizing inflammatory immunocyte infiltration to some extent. As one of the major components of extracellular matrix (ECM), HA has been widely used in biomaterials for treatment of central nervous system diseases [40]. Herein HA was modified with MA to allow gelation with HBPAK, whose structure was confirmed by $^1$H NMR (Fig. S1a). According to a previously reported calculation formula, the double bond grafting ratio of HA-MA ($X$) was calculated as $X = \frac{3A_1}{8A_2 - 12A_1}$, where $A_1$ represents the integral area of $^1$H from the carbon-carbon double bond at 5.5–6.5 ppm while $A_2$ represents the methyl at 1.5–2.2 ppm. Thus, the double bond grafting ratio of the HA-MA was 57.9 ± 4.61%, suggesting a over two double bonds were grafted in each HA structural unit.

After SCI, a series of inflammatory cascades were involved, especially the cellular damage under oxidative stress. To improve the

protection effect for endogenous neural cells, a ROS-scavenging HBPAK was used as the other component of the hydrogel. The HBPAK was synthesized by Michael additional between amine groups on ROS-responsive thioketal (TK) and double bonds on PEGDA575, whose structures were confirmed by $^1$H NMR (Figs. S1b and c). The molecular weight of HBPAK (Mn) was 4.8 kDa, Table S2).

Furthermore, a neural cell-adhesive peptide CQAASIKVAV was introduced to the HA-MA/PEGDA and HA-MA/HBPAK hydrogel by a one-pot mixing method. The IKVAV peptide has the function of neurogenesis-promotion and is widely used in treatment of central nervous system (CNS) diseases. Under the photoinitiation of LAP, the mixture solution of HA-MA, HBPAK and CQAASIKVAV peptides was gelated within 30 s to obtain the THI hydrogel. During this process, the cysteine-containing CQAASIKVAV was conjugated onto the HA-MA and HBPAK through the click-reaction between thiols and double bonds. Similarly, the non ROS-responsive IKVAV-peptide modified hydrogel (PHI hydrogel) was prepared. To confirm the conjugation of IKVAV peptides, the extracts from the THI hydrogel and the PHI hydrogel were measured by HPLC (Fig. S2a), suggesting no leachable IKVAV peptides from the hydrogels. A further DTNB detection for thiols (Fig. S2b) found no significant difference between the extract solutions of THI hydrogel and TH hydrogel (without CQAASIKVAV). These results confirm the chemical grafting of CQAASIKVAV peptides rather than physical encapsulation.

A matched mechanical property to the self-tissue would avoid secondary injury and inflammation caused by mechanical stimulation [41]. Generally, a hydrogel with a modulus similar to the spinal cord (100–3000 Pa) [42] is in demand. Rheological test found that the THI hydrogel with 10% HBPAK had a $G'$ larger than 300 Pa (Fig. S3 a,b). A larger concentration of HBPAK would also offer a better anti-oxidation property. Therefore, 10% HBPAK was used to prepare the TH, THI and THIEF hydrogels. The mechanical property of a hydrogel can also affect cell viability, proliferation, differentiation and stemness. According to the compression modulus (Fig. S3 c,d), 0.6% PEGDA was selected to prepare the non ROS-responsive PHI hydrogel. Both the time-sweep (Fig. 1 a1) and frequency-sweep (Fig. 1a2) tests showed that the $G'$ and $G''$ of the TH, THI, PH and PHI hydrogels were almost unchanged, suggesting all the hydrogels can maintain their integrity and robustness at the measuring conditions. The larger $G'$ than $G''$ reveals the gelation state. The $G'$ of both THI and PHI hydrogels was similar with a value higher than 1000 Pa, which was larger than that of the hydrogels without peptides. Due to the spatial hindrance, only some of the carbon-carbon double bonds can be crosslinked. The grafted peptides may enhance the intermolecular interactions by additional hydrogen bonding and charge interaction [43], resulting in hydrogels with larger mechanical strength.

Next, the degradation of PHI and THI hydrogels was monitored in PBS and 200 μM $H_2O_2$ solution (Fig. 1b). The THI hydrogel had a faster degradation in 200 μM $H_2O_2$ solution than in PBS, leading to about 51% and 35% weight loss 7 days later, respectively. The THI gel in 200 μM $H_2O_2$ solution was solubilized between day 9 to day 12, whereas lost 45% weight at day 15 in PBS. To identify the degradation products of the ROS-scavenging hydrogel, the lyophilized products of THI gel in PBS for 5 days was subjected to $^1$H NMR characterization. The characteristic

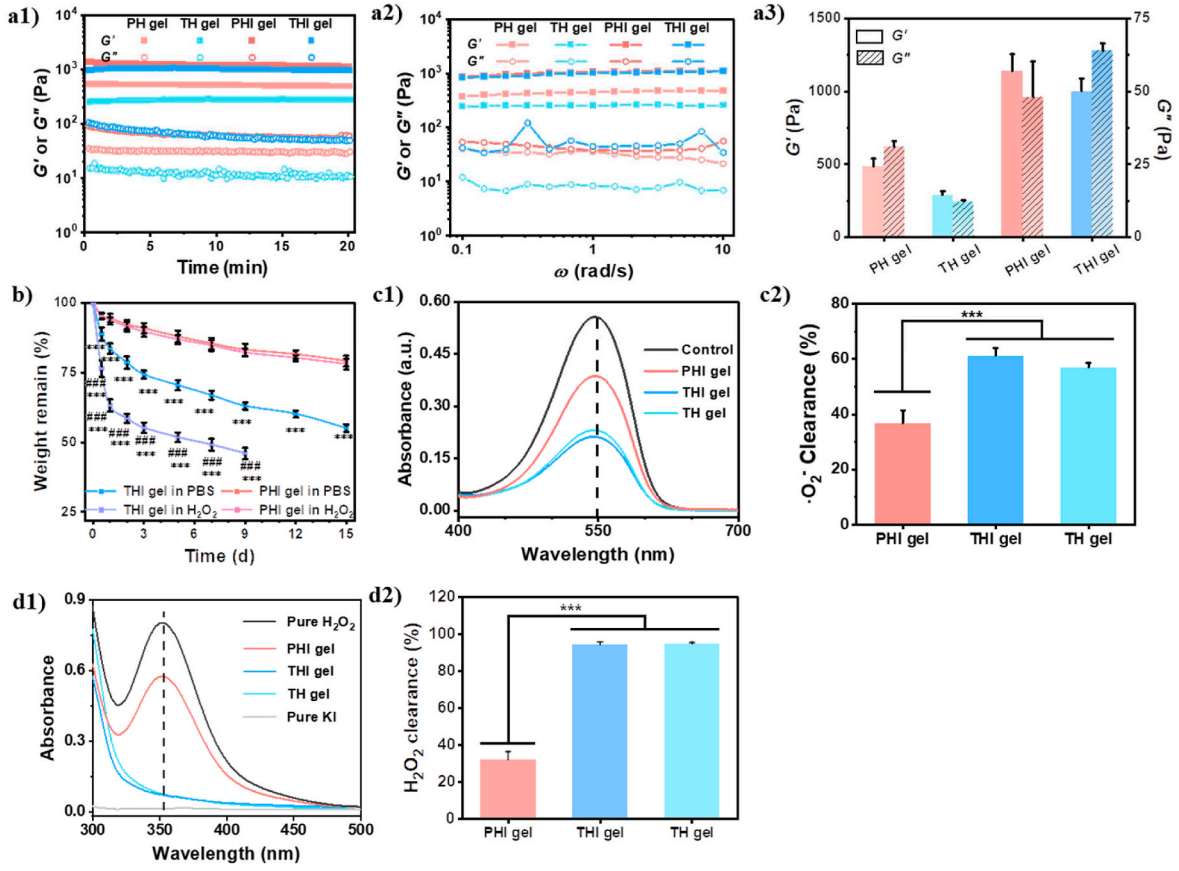


**Fig. 1.** Properties of different types of hydrogels. (a) Oscillatory tests as a function of (a1) time and (a2) frequency, and (a3) $G'$ and $G''$ measured thereof. The strain and temperature were kept as 1% and 37 °C for the time and frequency sweep tests, respectively, and the frequency was maintained at 6.28 rad/s for the time sweep. (b) Degradation of THI hydrogel and PHI hydrogel in 200 μM $H_2O_2$/PBS and pure PBS at 37 °C. (c,d) ROS-scavenging properties of HBPAK-containing THI hydrogels and their elimination efficacy, including (c1)·$O_2^-$ scavenging properties and (c2) its quantitative analysis of elimination efficiency, (d1) $H_2O_2$ elimination properties by using $H_2O_2$-KI assessment and (d2) its quantitative analysis of elimination efficiency. The HBPAK, PEGDA, HA-MA and LAP concentrations were kept at 10% w/v, 0.6% w/v, 1% w/v, and 0.05 w/v, respectively to prepare the corresponding hydrogels.

peaks at the 5.8 ppm–6.5 ppm, 1.7 ppm and 2.2 ppm (Fig. S4) indicate the existence of the double bonds, the methyl groups and the acetone, respectively. The existence of acetone suggests the thioketal destruction of the THI gel as well. The absence of ~5.0 ppm peak excludes the existence of HA-MA component. The singlet peak of the methyl group is attributed to the thioketal structure, which also suggests the degradation of the β-amino ester bonds. Therefore, the hydrolysis of β-amino ester bonds in HBPAK is the main reason for degradation of THI gel in PBS [33]. The degradation profiles of PHI hydrogel had no significant difference in 200 μM $H_2O_2$ and PBS, and totally about 21% weight loss was found after incubation for 15 days. These results are in good agreement with the faster degradation of a hydrogel or scaffold prepared by ROS/RNS scavenging and stimuli-responsive biopolymers [44], which is believed to avail stemness maintenance and neural differentiation of the encapsulated stem cells [45,46].

The anti-oxidation and anti-radical properties of different hydrogels were compared by scavenging DPPH, $H_2O_2$, and·$O_2^-$. Compared to the PHI hydrogel, the THI and TH hydrogels exhibited stronger scavenging of both $H_2O_2$ and·$O_2^-$ (Fig. 1c, d), due to the existence of HBPAK component (Fig. S5a). The HA-MA has anti-oxidation ability to some extent [47]. The PHI hydrogel, and TH and THI hydrogels could clear about 38% and 60% ·$O_2^-$ (Fig. 1c), respectively. More apparently, the TH and THI hydrogels cleared almost all $H_2O_2$ while the PHI hydrogel decomposed only 30% (Fig. 1d). It has to mention that the incorporation of CQAASIKVAV peptides did not deteriorate the good anti-oxidation of TH hydrogel (Fig. 1c,d and Fig. S5c). The THI hydrogel exhibited great scavenging effect for DPPH free radicals, which were eliminated within about 7.5 h (Fig. S5c). Although the final content of HBPAK was same, the soluble HBPAK would be easier to react compared with that in the hydrogel due to the less diffusion restriction. For hydrogel, the DPPH radicals need to penetrate into the hydrogel network before they can react with the thioketal linkages.

### 3.2. Antioxidation and protection effects of hydrogels in vitro

It has been widely accepted that the transplantation of stem cells is helpful in axon regeneration in CNS-related diseases. Herein, encapsulation of stem cells was proposed in the design of our SCI-therapy system. Besides, EGF can maintain the renewal of BMSC without inducing their differentiation *in vitro* [48]. However, several studies prove that BMSCs would turn into the neural progenitor-like cells in the presence of bFGF and EGF [49]. Moreover, the simultaneous delivery of EGF and bFGF *in vivo* results in the significantly greater proliferation of ependymal cells in the central canal, which migrate to the rostral and caudal sites [50], and increase the axon growth [51]. Therefore, EGF and bFGF were introduced to the THI hydrogel to obtain the THIEF hydrogel.

The cytotoxicity of TH, PH, THI and PHI hydrogels was determined by culture of Schwann cells (Fig. S6a) and BMSCs (Fig. S6b) with their extracts, followed by CCK-8 assay. The cell viability of all hydrogel groups was nearly 100% compared to the control, suggesting no cytotoxicity. These results were further substantiated by PicroGreen DNA proliferation measurement (Fig. S6c), excluding possible interference of redox substances to the CCK-8 assay too. Moreover, the relative viability of BMSCs being co-cultured with the extracts of different hydrogels collected at day 3 and day 7 was over 90% (Fig. S6 d,e), suggesting neglectable cytotoxicity of the degradation products. In addition, the BMSCs were encapsulated in the TH, PH, THI, PHI, THIEF and PHIEF hydrogels and cultured for 1–5 days, respectively, followed by Live/Dead staining (Fig. 2a–c and Fig. S6f). All groups had live cell percentages over 70% without significant difference and change over time at

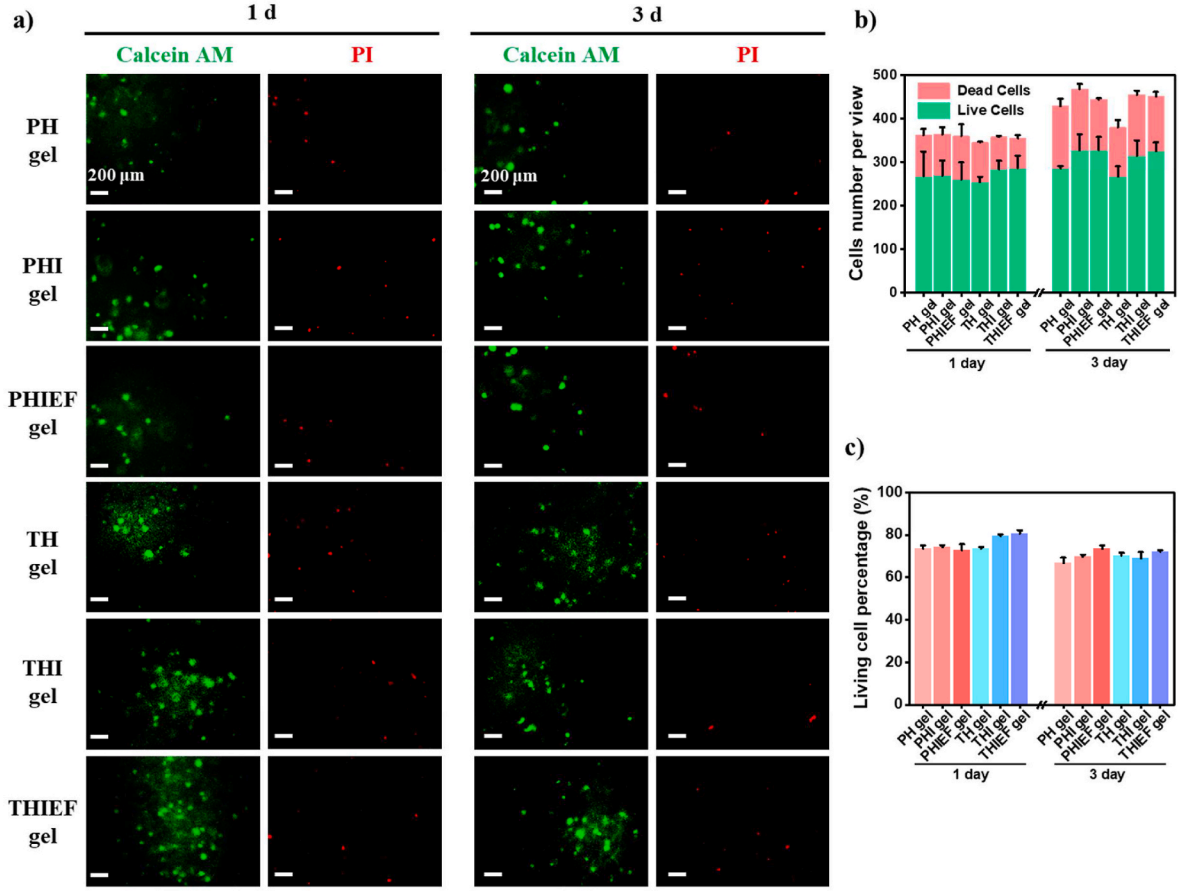


**Fig. 2.** Cytotoxicity and cytocompatibility of different hydrogels. Calcein AM and propidium iodide (PI) Live/Dead staining on BMSCs encapsulated in different hydrogels with a density of 8 × $10^6$ per mL post culture for (a) 1 day and 3 days. Quantitative analysis of (b) cell numbers and (c) living cell percentages.

day 1 and day 3 (Fig. 2b and c). It is known that the PEG and HA-based hydrogels usually possess good biocompatibility. Hence, the death or damage of encapsulated cells is most likely attributed to the difficulty in infiltration of nutrition and oxygen, insufficient cell-matrix interactions, and UV exposure during gelation.

To study the protection effect of ROS-scavenging hydrogel from oxidative damage *in vitro*, the macrophages were stimulated into the inflammatory phenotype under LPS and IFN-γ induction in the lower Transwell chamber. Meanwhileonto the upper chamber the hydrogel-encapsulated BMSCs were placed (Fig. 3a). Live/Dead staining (Fig. 3b,**c)** shows that the THIEF-Cell group had significantly larger percentage of live cells (65.6 ± 4.0%) compared to the PHIEF-Cell group (47.3 ± 2.9%), which is only slightly smaller than that being cultured under normal conditions (70%, Fig. 2c2). This result reveals that the viability of BMSCs is indeed influenced significantly by the inflammatory macrophages, and the THIEF can efficiently alleviate the hostile microenvironment and protect BMSCs.

Moreover, the influence of hydrogels and BMSCs on the stimulated macrophages was measured (Fig. 3a). After stimulation, the DCF fluorescence intensity was significantly enhanced as shown by the offset of the peak, and the emerge of the second peak represents the strong positive staining (Fig. 3d). By applying the hydrogels, BMSCs or their composite materials, the intracellular ROS production was significantly reduced, as shown in the significantly decreased DCF fluorescence intensity and the gradually vanished DCF positive peak (Fig. 3d and e). Particularly, pure 2D culture of BMSCs exhibited a similar endogenous ROS scavenging efficacy in comparison to the ROS-scavenging THIEF hydrogel, as confirmed by the parallel $DCF^+$ cell percentage (20.3 ± 0.7% for 2D BMSCs and 19.8 ± 0.7% for THIEF hydrogel vs 59.5 ± 0.5% for the stimulated macrophages) and the mean fluorescence intensity (MFI) (117.5 ± 3.4 for 2D BMSCs and 107.0 ± 3.2 for THIEF hydrogel vs 408.0 ± 2.6 for the stimulated macrophages). The encapsulated BMSCs and ROS-scavenging hydrogel exhibited the strongest effect on reducing intracellular ROS production in macrophages. Similarly, pure 2D culture of BMSCs exhibited a parallel reduction of CD86 marker on the surface of Raw 264.7 cell membrane in comparison to the ROS-scavenging

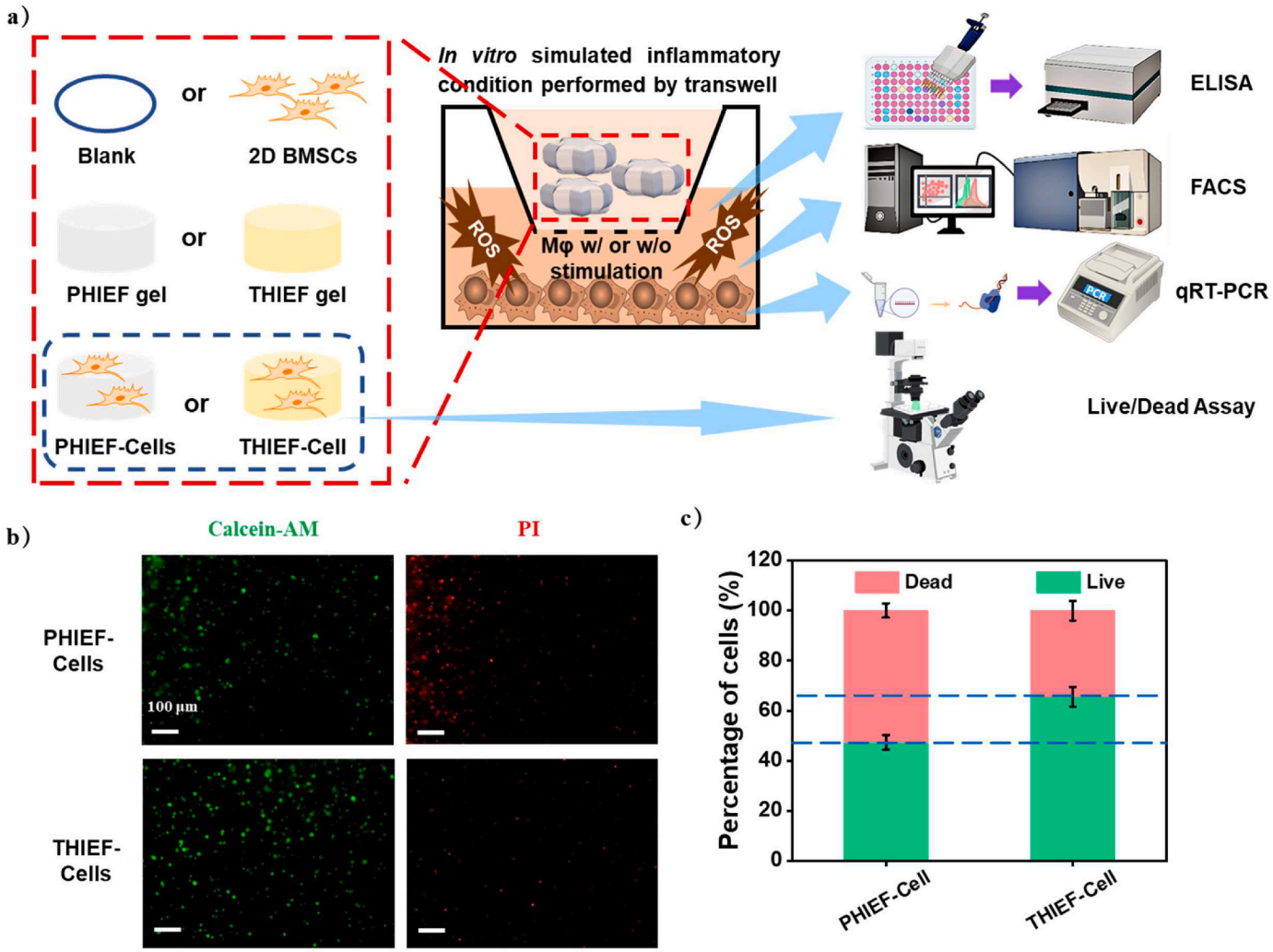


**Fig. 3.** *In vitro* simulated environment of inflammation and oxidative damage performed by co-culturing in a Transwell chamber, including protection of ROS-scavenging hydrogel towards the encapsulated BMSCs. (a) Schematic illustration of the simulated inflammation model and co-culture of cells at different conditions *in vitro*, including hydrogels with or without BMSCs encapsulation, pure 2D culture of BMSCs in the upper chamber and the stimulated Raw 264.7 in the lower chamber, and their characterization methods. (b) Calcein AM and PI Live/Dead staining on encapsulated BMSCs in THIEF and PHIEF hydrogels for 1 day to evaluate the viability in oxidative condition. (c) quantitative analysis of live cells. (d–g) Flow cytometry and histograms of (d, e) DCF and (f, g) FITC fluorescence intensity of the DCFH-DA or FITC-anti-mouse-CD86 stained Raw 264.7, including (e1) mean DCF fluorescence intensity, (e2) $DCF^+$ cell percentage, (g1) mean FITC fluorescence intensity and (g2) $CD86^+$ cell percentage. (h,i) Expression levels of pro-inflammatory (h) IL-6 and (i) TNF-α tested by ELISA assay in the supernatant of Raw 264.7 medium from each group collected at 1 day after co-culture. (j–l) Transcription levels of pro-inflammatory (j) CD86, (k) IL-6 and (l) TNF-α tested by qRT-PCR assay in the harvested Raw 264.7 at 1 day after co-culture. Data are presented as mean ± SD (n = 4).

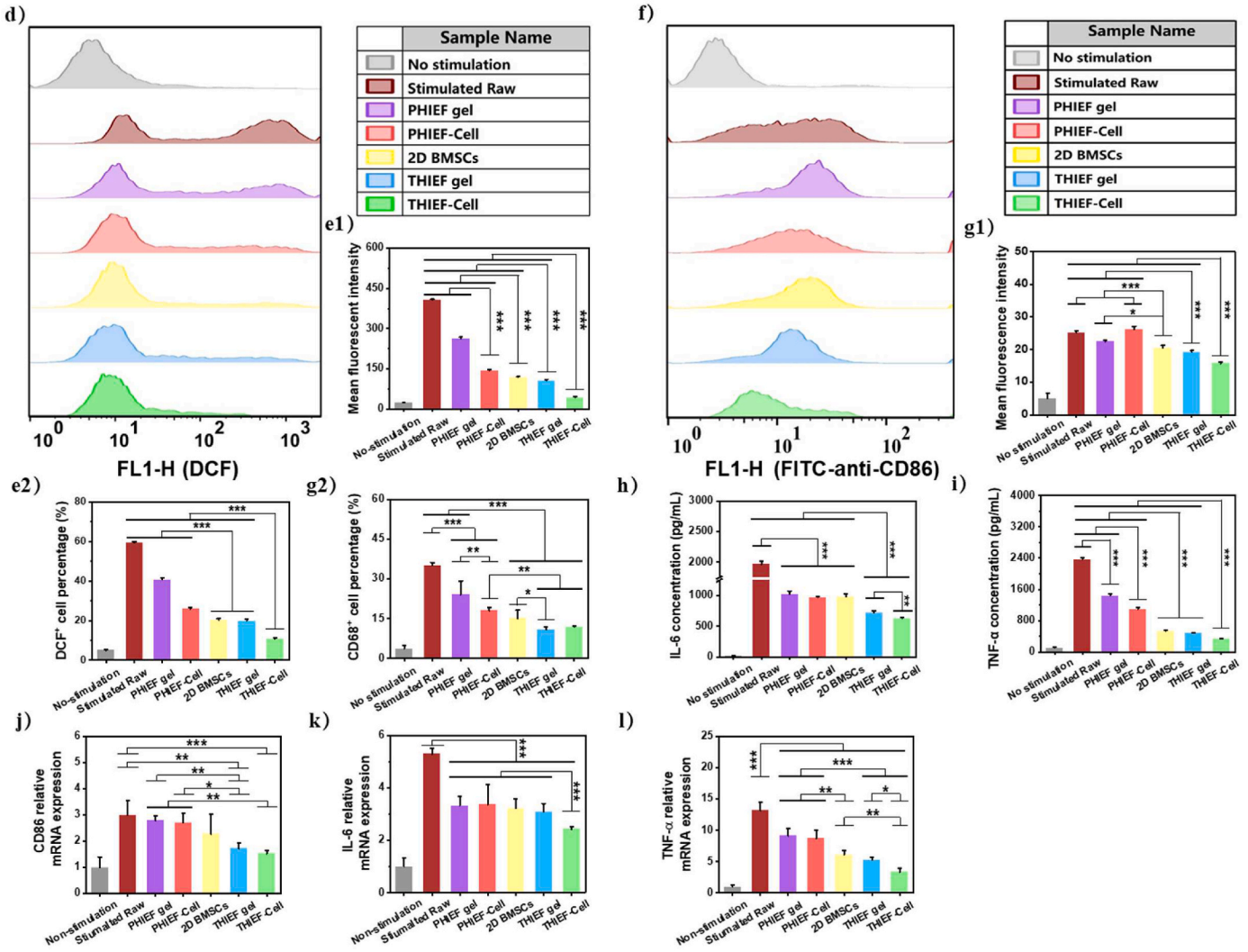


**Fig. 3.** (*continued*).

THIEF hydrogel, as suggested by the similar $CD86^+$ cell percentage and the MFI of FITC-labeled anti-CD86 anti-body(Fig. 3f and g).

It was reported that in LPS-induced RAW264.7 macrophages, the activated TLR4 and NOX2 would lead to ROS overproduction, together with nuclear factor-κB (NF-κB) translocation from the cytoplasm to the nucleus, in which case the pro-inflammatory mediators such as TNF-α and IL-6 would be up-regulated [52]. The concentrations of IL-6 and TNF-α were significantly reduced in the supernatants of 2D cultured BMSCs and the ROS scavenging hydrogel groups, with a synergetic effect when both existed (Fig. 3h and i). These results are further substantiated by the transcription levels of CD86, IL-6 and TNF-α as shown by the qRT-PCR (Fig. 3j,k,l).

The BMSCs are known to possess the immune-modulating property, which may stimulate other cells to produce hydrogen peroxide scavenging enzymes and fight against oxidation stress [53–55]. BMSCs could alleviate the pro-inflammatory polarization of macrophages and promote the pro-regenerative polarization by secretion of TGF-β [56], which can be upregulated under the stimulation of TNF-α [57]. BMSCs would present as the inflammation-suppressive and pro-trophic phenotypes under the stimulation of IL-1 [58].

Although the ROS-scavenging hydrogels existed in the cell culture medium merely reacted with the extra-cellular $H_2O_2$, the endogenous ROS were significantly reduced. The pro-inflammatory immune cells will overproduce ROS to the tissue microenvironment, which serve as the danger-associated molecule pattern (DAMP) to recruit more immune cells through ROS/MAPK/NF-κB/p65 signal pathway and launch the nucleus translocation of NF-κB, so that a new round of inflammatory cytokines transcription starts [59,60]. As a result, more immune cells are activated. Meanwhile, the transcription and expression of nuclear factor erythroid-2 related factor 2 (Nrf2), together with the anti-oxidant proteins regulated by Nrf-2, such as the NAD(P)H quinone oxidoreductase 1 (NQO1) and glutathione S-transferases (GST), will be down-regulated to decrease the endogenous redox biomolecules [24,61,62]. On this account, more endogenous and intracellular ROS will be produced. By contrast, the scavenging of extracellular ROS will result in the alleviation of oxidation stress, leading to the reduction of the intracellular ROS.

Therefore, it can be safely concluded that the BMSCs-encapsulated ROS-scavenging hydrogel provides strong anti-inflammation by ROS-scavenging and immune cell-regulation.

### 3.3. Antioxidation in vivo

The massive ROS (especially the $\cdot O_2^-$ and $H_2O_2$ [63]) uncontrollably overproduced by the infiltrated neutrophils and macrophages and the dysfunctional mitochondria in the injured neural cells would greatly contribute to the oxidative damage of DNAs, proteins and lipids [64], leading to secondary death of neural cells. The ROS-scavenging biomaterials could eliminate the overproduced ROS via the changes of their hydrophobic and hydrophilic performance and the breakdown of the covalent bonding or the ion valence, which is helpful in maintaining the

equilibrium of endogenous redox systems [65]. In SCI cases, the over-produced ROS are closely interrelated to the overload of both $Ca^{2+}$ and glutamate, which synergistically contribute to the apoptosis and necrosis of both neurons and gliocytes.

To assess the *in vivo* therapeutic efficacy of our hydrogels, a rat T10 transection SCI model with a lesion gap of 2 ± 0.5 mm was constructed. The BMSCs-encapsulated thioketal-containing and IKVAV peptide-modified ROS-responsive hydrogel (THIEF-Cell) was implanted into the lesion gap immediately after transection, with the BMSC-encapsulated PEGDA-containing and IKVAV-modified non-ROS responsive hydrogel (PHIEF-Cell), pure IKVAV-containing ROS-responsive hydrogel (THI hydrogel), as well as transection without any treatment (SCI group) as the controls (Fig. 4a).

The antioxidation and anti-inflammation properties of the THIEF hydrogel was then investigated *in vivo* 7 days post-surgery. The intracellular $\cdot O_2^-$ level was significantly decreased in the spinal cord tissue, especially at the lesion site, after implantation of the THI hydrogel and THIEF-Cell compared to the PHIEF-Cell or the blank SCI control groups, as revealed by both the cell fluorescence distribution at the lesion site and the mean fluorescence intensity of dihydroethidium (DHE) staining (Fig. 4b–d). Specifically, the mean fluorescence intensity of the THI hydrogel and THIEF-Cell groups were 18.8 ± 1.2 and 20.8 ± 0.8, respectively, which were significantly ($p < 0.001$) smaller than that of the PHIEF-Cell group (30.2 ± 1.0) and SCI group (44.0 ± 1.2). Apart from intracellular ROS, the immunofluorescence staining of the oxidative DNA damage marker 8-hydroxy-2′-deoxyguanosine (8-OHdG) (Fig. 4e) was also performed, and the corresponding cell fluorescence distribution at the lesion site and the average ratio of the 8-$OHdG^+$ area were calculated (Fig. 4f and g). Both the THI hydrogel and THIEF-Cell group had a less fluorescence intensity and a narrower distribution compared to the PHIEF-Cell and SCI groups. Besides, Fig. 4g shows that the 8-$OHdG^+$ area ratios of the THI hydrogel (17.0 ± 3.4) and the THIEF-Cell (16.7 ± 4.8) group were significantly smaller than those of the PHIEF-Cell (30.0 ± 5.2) and the SCI group (29.1 ± 7.2) ($p < 0.001$), suggesting a reduced DNA damage as a result of the ROS-scavenging efficacy. Herein, the oxidative progress of these cellular components was greatly prevented. The THI hydrogel in this study has shown its great antioxidation against DPPH radical, $\cdot O_2^-$ and $H_2O_2$ *in vitro*, which

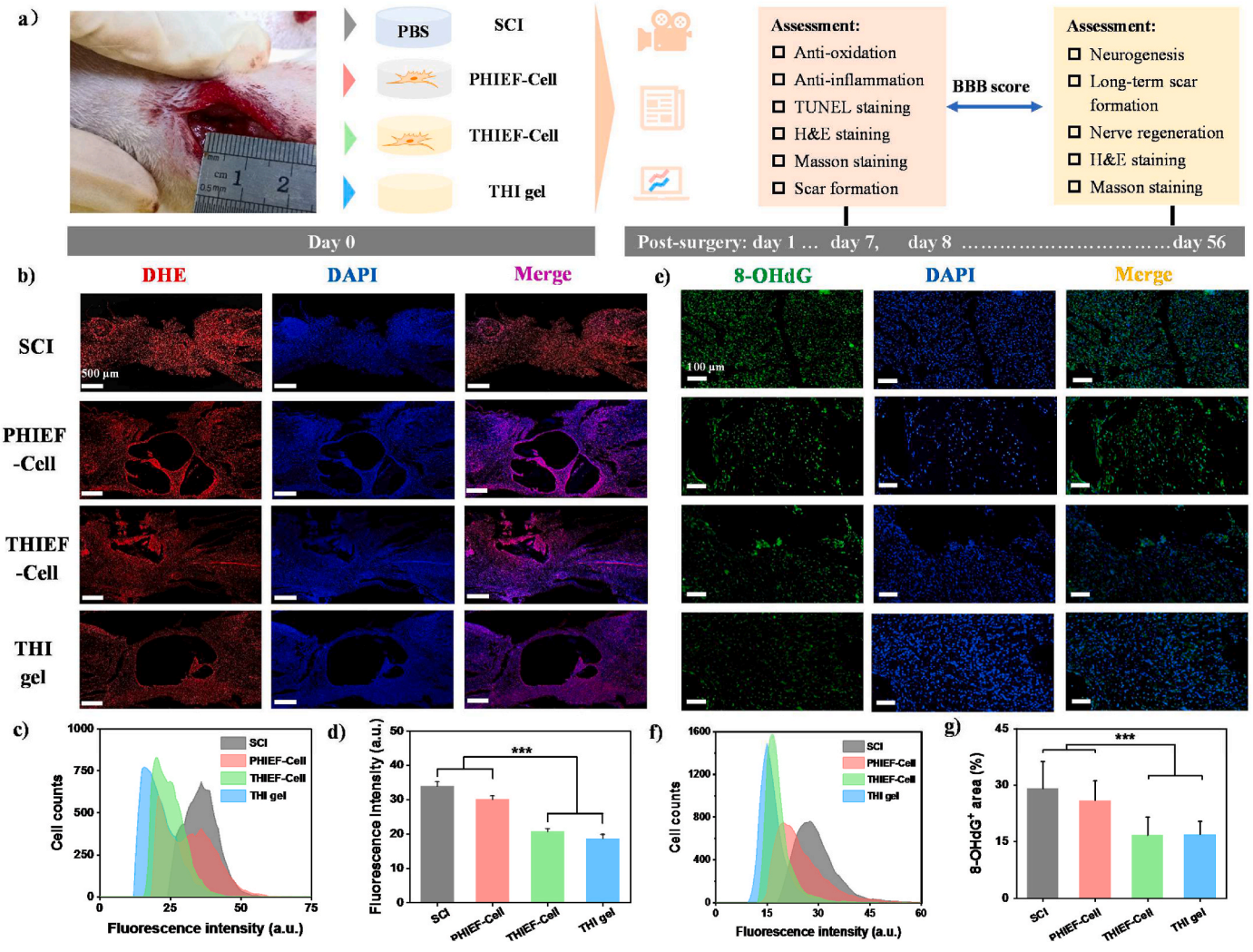


**Fig. 4.** (a) Schematic illustration to show the implantation of BMSC-encapsulated non ROS-responsive hydrogels (PHIEF-Cell), BMSC-encapsulated ROS-responsive hydrogels (THIEF-Cell) and ROS-responsive hydrogel (THI hydrogel) into rats with a 2.0 mm spinal cord transection, and analysis of their antioxidation effects post surgery for 7 days. (b~d) Dihydroethidium (DHE) staining showing the superoxide anion levels at the lesion site *in vivo*. (b) Corresponding representative micrographs, together with (c) their histograms showing the fluorescence intensity, and (d) the mean fluorescence intensity calculated from 9 fluorescence images. (e~g) Immunofluorescent staining of oxidative DNA damage products 8-hydroxy-2′- deoxyguanosine (8-OHdG) at the lesion site of the spinal cord tissues, suggesting the effective antioxidation and protective functions of the HBPAK-containing ROS-responsive hydrogel *in vivo*. Extent of oxidative damage was analyzed in terms of histogram of (f) the fluorescence intensity and (g) mean 8-OHdG positive area calculated from 9 micrographs (size: 1920 × 1080 pixels) from at least 3 sections for each group. Data represent as mean ± SD. ***$p < 0.001$.

explains the good antioxidation results *in vivo*.

### 3.4. Anti-inflammation and anti-apoptosis in vivo

The macrophages recruited by the chemokines participate in the secondary injuries in the lesion site and take control in the repair and regeneration process [66]. Although there may exist a continuum between M1 and M2, a M1 phenotype represents a pro-inflammatory type and a M2 phenotype stands for an anti-inflammatory type [67]. In general, the M1 macrophages will secret multi-types of inflammatory cytokines such as IL-1β, IL-6 and TNF-α to recruit infiltration of peripheral immune cells, and thus aggravate the secondary injuries, whereas the M2 macrophages will produce numerous pro-regenerative cytokines to accelerate repair and regeneration. Moreover, the over-produced ROS by inflammatory immune cells can act as molecular pattern that triggers downstream MAPK/JNK/NF-κB p65 signal pathway, and thereby promotes the expression of inflammatory cytokines [23,68], leading to the secondary death of neural cells, including ferroptosis, pyroptosis and apoptosis [69,70]. In reference to the TNF-α, a network analysis involving >10,000 genes associated with SCI reveals that it functions as a major hub of reactive inflammation following SCI. Along with other hubs such as MMP-9, IL-6 and TGFBR, TNF-α is involved in cellular responses and metabolic processes in extracellular space and extracellular region components, in protein-binding and receptor-binding functions as well as in the TNF signaling pathway [71]. Besides, there exist tremendous changes of local and systemic IL-1β after SCI [72], which participate in the classical and alternative activation of microglia/macrophages [73]. Moreover, IL-1β is believed to take part in the activation of highly-inflammatory pyroptosis after SCI [70]. As a representative marker during the acute inflammation, IL-6 promotes the NSCs differentiation into astrocytes and inhibits the neuron differentiation [74].

Therefore, the anti-inflammation efficacy of our hydrogels was investigated. Immunofluorescence staining of CD86 (M1 marker) and CD163 (M2 marker) was applied to show the macrophage infiltration and polarization (Fig. 5a). Fig. 5a1 shows that the $CD86^{+}$ cells were diminished in the THI hydrogel and THIEF-Cells group, whereas remained unchanged in the PHIEF-Cell group compared to the SCI control, suggesting a decrease of M1 phenotype in the ROS-scavenging hydrogels. By contrast, the intensity of $CD163^{+}$ area was enhanced in both the THI hydrogel and THIEF-Cell group, indicating an increase of M2 phenotype. Further quantitative analysis shows that the M2/M1 ratios in the THIEF-Cell group and the THI hydrogel were 2.76 ± 0.48 and 2.42 ± 0.55 folds to that in the SCI group (Fig. 5a2).

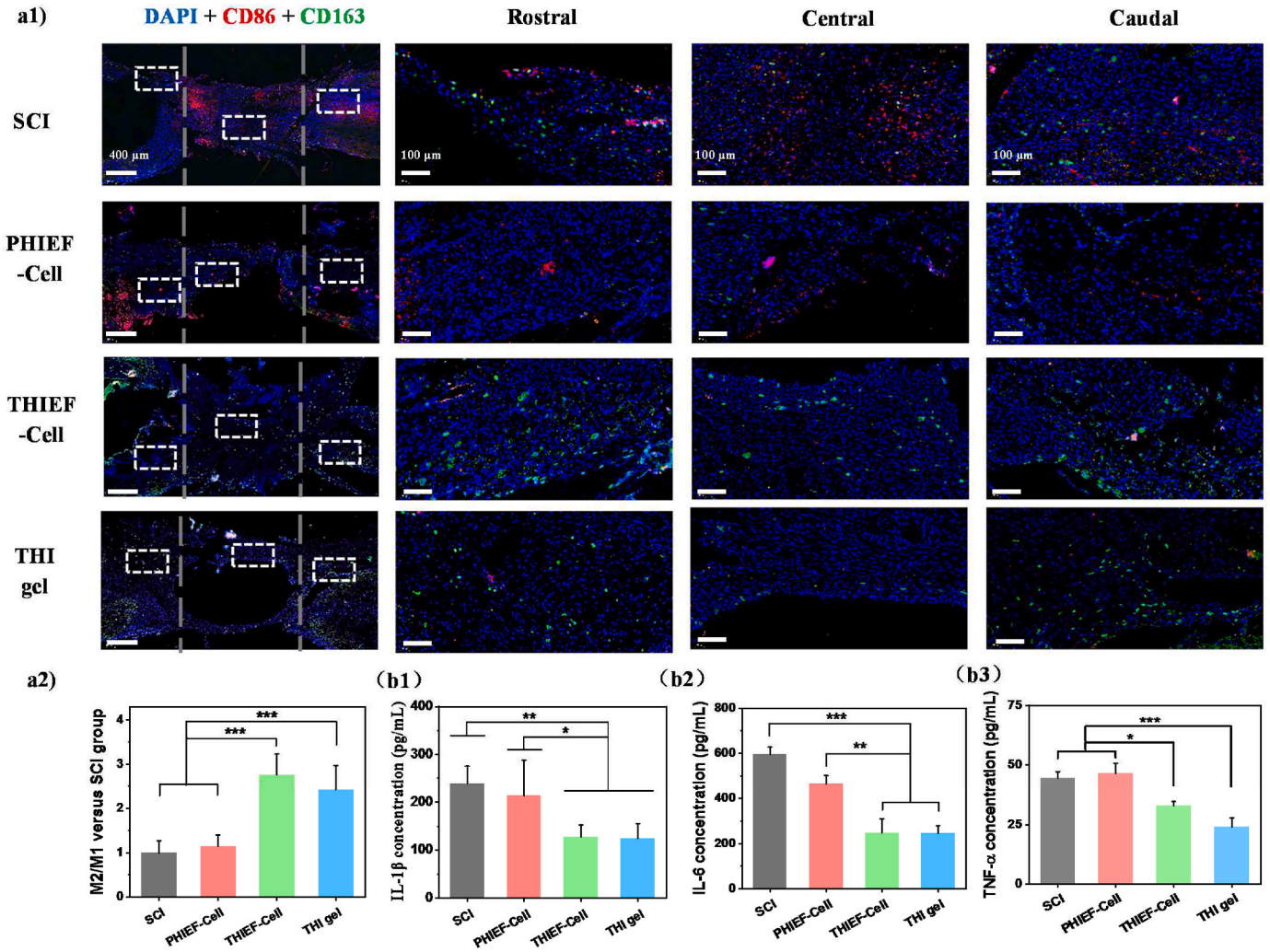


**Fig. 5.** Assessment of anti-inflammatory properties of BMSC-encapsulated ROS-responsive hydrogel post implantation for 7 days in rats with 2.0 mm spinal cord transection. (a1) CD86 (M1 marker) and CD163 (M2 marker) double immunofluorescence staining images, and magnified images in the white box regions, respectively. (a2) M2/M1 ratio determined at the lesion sites. (b) ELISA assay of inflammatory cytokines collected at tissue supernatants for (b1) IL-1β, (b2) IL-6 and (b3) TNF-α. (c) H&E staining images of rat spinal cord tissues at the lesion sites post treatment for 7 days *in vivo*. The distance between two grey dashed lines in the first panel outline the 2.0 mm gap. $^{*}p < 0.05$, $^{**}p < 0.01$, $^{***}p < 0.001$.

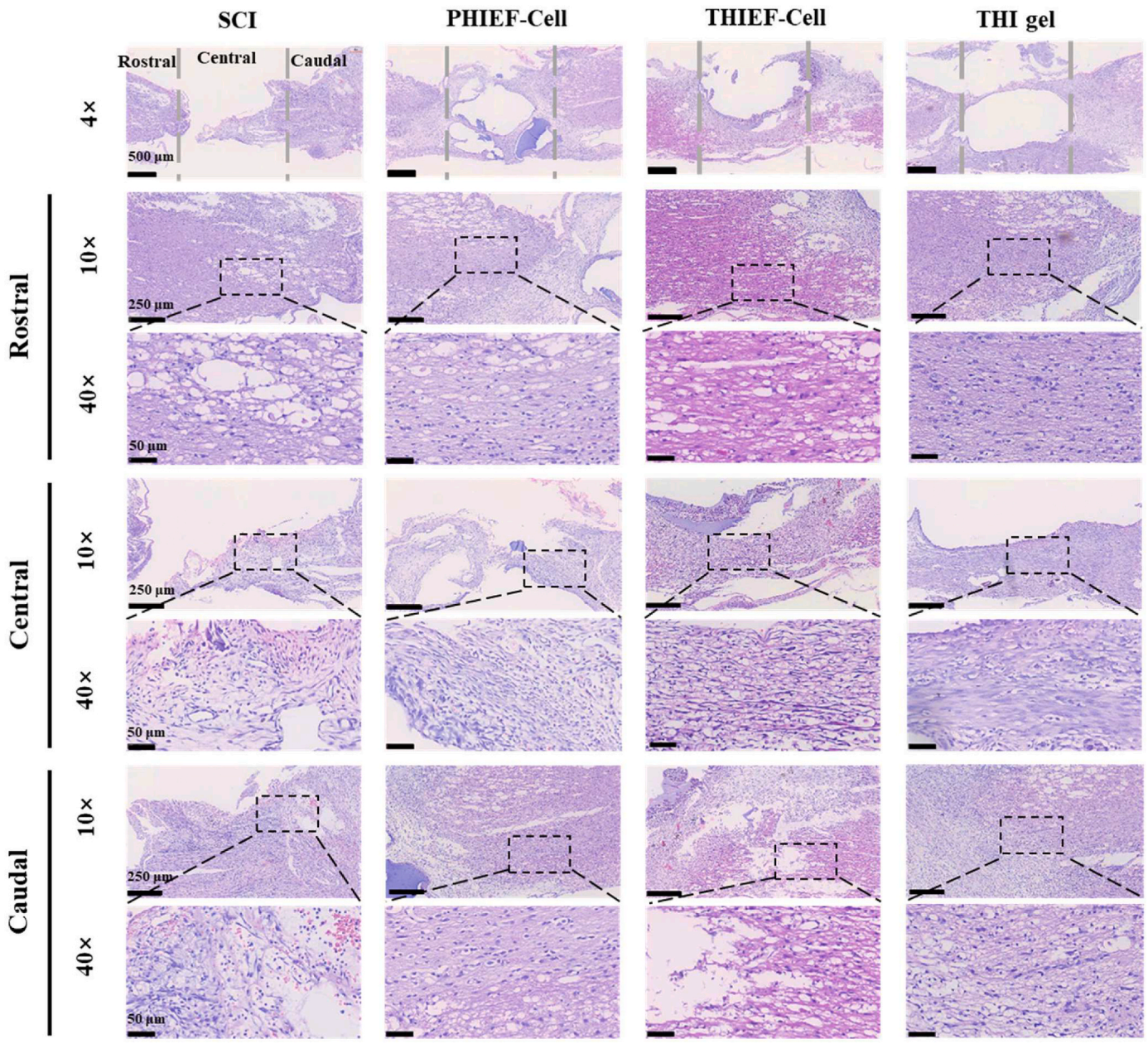


**Fig. 5.** (*continued*).

The expression of key inflammatory cytokines in the spinal cord tissue homogenate was measured by ELISA (Fig. 5b). The ROS-scavenging THI hydrogel and THIEF-Cell could significantly reduce the concentrations of L-1β, IL-6 and TNF-α, whereas the PHIEF-Cell only had minor effect on reducing the IL-6 expression compared to the SCI control group. A previous study shows that the transplantation of MSCs for SCI treatment would upregulate the gene expression of Caspase compared to the transplantation of other types of stem cells or even the SCI group [75]. The transcription of IL-1β and TNF-α at day 7 post-surgery shows no significant difference compared to the SCI group [75]. These results are consistent with our findings, i.e. no difference of the IL-1β and TNF-α concentrations between the SCI and the PHIEF-Cell group, and between the THIEF-Cell and the THI hydrogel group.

Furthermore, the H&E staining also confirms a decrease of the inflammatory leukocyte infiltration within the THI hydrogel and THIEF-Cell group (Fig. 5c). By contrast, many inflammatory immunocytes aggregated in the SCI group. All the results suggest that the acute inflammation was suppressed and the pro-regeneration effect was enhanced to some extent.

The excessive ROS can also activate the apoptosis signal pathway by destructing the afore-damaged mitochondria, leading to the leakage of pro-apoptotic cytochrome C that binds to the procaspase-9-bound Apaf-1. As a result, caspase-9, the apoptosis promotor, is activated to trigger the caspase cascade, resulting in the activation of apoptosis media caspase-3 and further amplifying the cascade [76]. On this account, a sharp increase of caspase-3, caspase-8 and caspase-9, downregulation of the anti-apoptosis protein B-cell lymphoma 2 (Bcl-2), and upregulation of the pro-apoptotic protein Bcl-2-associated x-protein (BAX), take place in the lesion site [77], leading to the widespread apoptosis of neural cells, especially the neurons [78]. Nissl staining was thus conducted to observe and evaluate the morphology of neuron cells at the similar position of the rostral and caudal sites. The neuron cells in the THI hydrogel and THIEF-Cell groups had more normal morphology and a greater number of Nissl body (Fig. S7a). By contrast, the number of Nissl body decreased, and the pyknotic nuclei were observed in the PHIEF-Cell and the SCI groups, indicating more neuron damages.

Moreover, TUNEL staining was performed to detect cell apoptosis. The mean apoptotic cell numbers in both the rostral and caudal sites in the THI hydrogel (86.6 ± 18.6) and THIEF-Cell group (85.1 ± 11.1) were significantly smaller than those in the PHIEF-Cell (122.1 ± 24.2) and the SCI group (132.9 ± 24.1) (Fig. S7b).

These results reveal that implantation of the ROS-scavenging THI hydrogel and THIEF-Cell can efficiently protect the neuron cells surrounding the lesion sites against apoptosis or damage caused by the excessive ROS-mediated secondary injuries. Therefore, more neural tissues were preserved to lay a solid foundation for the subsequent neurogenesis and/or neural repair.

### 3.5. Reduced fibrotic and glial scar formation

Currently it is still debating whether the scars are advantageous or disadvantages for the neural repair and axon regeneration [79]. Indeed, there are two major components in scars at different sites of an injured spinal cord. Generally, the fibrotic scars consist of inflammatory immunocytes and fibroblasts in the lesion site core, while the activated astrocytes interact with fibro meningeal cells and other gliocytes, contributing to the scar border known as penumbra or a glial scar [80]. Although the scar formation can block wound and injury from further expansion, it would set an obstacle for axon regeneration [81]. Moreover, the axon growth inhibitory ligands secreted from incipient scar, such as chondroitin sulfate proteoglycans, semaphorins and ephrins, can restrict the plasticity and axonal regeneration or mediate axon growth cone collapse [66]. On the other hand, the glial scar is also regarded as the result of regeneration failure but not the reason recently [82]. Nonetheless, the excessive scar formation at early stage is averse to neurogenesis and function restoration. The fibrotic scar is formed because of the inflammation and thus, making the microenvironment unsuitable for repair and regeneration [82]. Specifically, the activated microglia and macrophages in the lesion site would express large amount of integrin α5β1, the canonical fibronectin receptor, to mediate the assembly of fibronectin matrix, contributing to the accumulation of fibroblasts and the deposition of fibronectin that lead to the fibrotic scar formation [83].

Therefore, the regulation of scar formation is important for successful SCI treatment [84]. Masson staining was applied to stain the traumatic spinal cord tissue at day 7 (Fig. S8) and day 56 (Fig. S9) post-surgery. At day 7, a reduced scar and collagen deposition could be observed in the THIEF-Cell group, as shown by the less aniline blue positive area. At day 56, both the THIEF-Cell and the THI hydrogel groups showed less aniline blue positive areas and more purple-colored area in the lesion site, suggesting a less scar formation and more neural fiber perseveration. The formation of these two distinct scars at day 7 (Fig. 6) and day 56 post-surgery (Fig. S10) was then explored by immunofluorescence staining. The activated astrocytes labeled by GFAP contribute to the glial scars that penetrate through the lesion gap and form a harmful cavity [85]. Herein, PDGFR-β was selected as the marker of the fibrotic scars [86]. Thus, PDGFR-β/GFAP double staining was carried out. The quantitative analysis at 7 day (Fig. 6) shows that both the THIEF-Cell (10.0 ± 1.2%) and THI hydrogel groups (10.0 ± 1.5%) had significantly smaller percentage of the PDGFR-$\beta^+$ areas compared to the PHIEF-cell (14.8 ± 2.1%) and SCI groups (16.5 ± 2.3%). Similarly, the reduced percentages of the $GFAP^+$ areas were observed in the THIEF-Cell (1.8 ± 0.8%) and THI hydrogel groups (1.9 ± 0.9%) compared to the other two groups (5.6 ± 1.9% and 3.6 ± 1.4%, respectively). Taken together, the ROS-scavenging hydrogel, no matter with or without BMSCs encapsulation, could significantly reduce the formation of both fibrotic and glial scars in the lesion site, which is important for axon regeneration.

The reduced infiltration of inflammatory immunocytes has been proved to efficiently alleviate the fibrotic scar formation. For instance, reduced macrophage infiltration by hematogenous macrophage depletion decreases the fibrotic scar [87]. Moreover, the inflammatory immunocyte-regulating biomaterials, such as laponite nanoparticles [88] and F127-polycitrate-polyethyleneimine hydrogel [89], can minimize the macrophage infiltration, and thus diminish the fibrotic scar formation. In this study, the THIEF-Cell and the THI groups can successfully regulate the secondary inflammation via promotion of the macrophage polarization and downregulation of the inflammatory cytokines such as IL-1β, IL-6 and TNF-α. On this account, the fibrotic scar formation is attenuated. The good biocompatibility of our hydrogels is also helpful to attenuate the glial scar formation. These results indicate the promising application of our ROS-responsive hydrogel in nerve tissue repair post SCI.

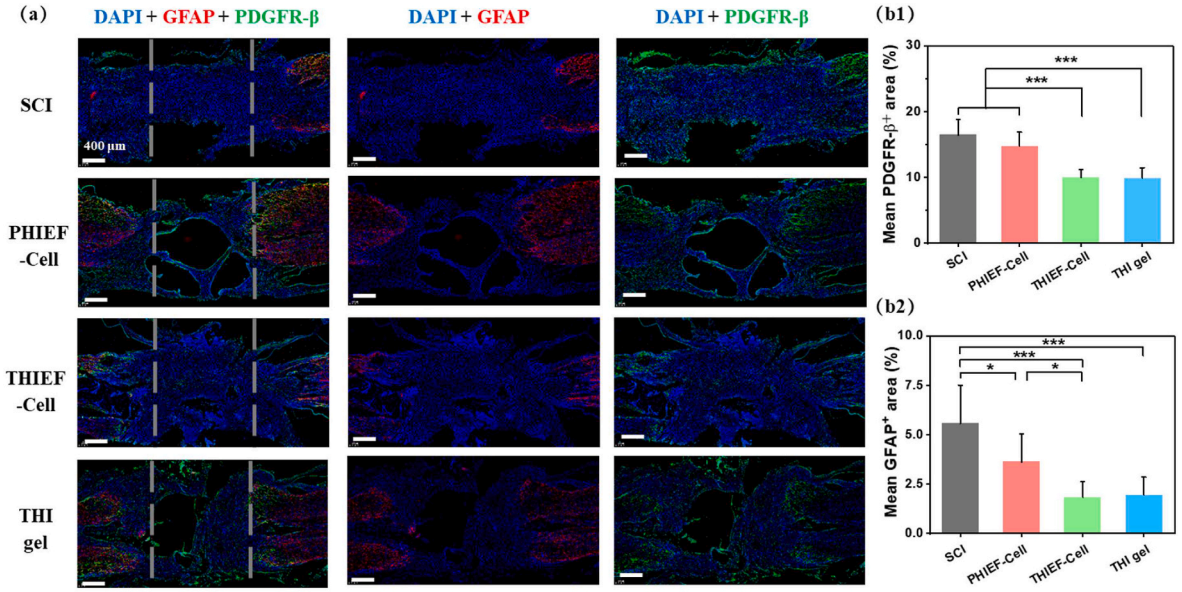


**Fig. 6.** Assessment of formation of both fibrotic scar and glial scar. (a) PDGFR-β (platelet-derived growth factor receptor-β, fibrotic scar marker) and GFAP (glial fibrillary acidic protein, glial scar marker) double immunofluorescence staining of spinal cord tissues at the lesion sites. (b) quantitative analysis of scaring levels by (b1) PDGFR-$\beta^+$-positive area and (b2) $GFAP^+$-positive area. The dashed lines outline the 2 mm lesion sites.

### 3.6. Neurogenesis, axon regeneration, and motor recovery in vivo

After severe transection, the rats without any treatment (SCI group) exhibited very limited motor behaviors, whereas a better motor recovery was observed in the THIEF-Cell group, with a significantly improved Basso-Beattie-Bresnahan (BBB) score (7.5 ± 1.5) compared to the SCI group (4.9 ± 1.2) on day 56 post-surgery, and an enhanced BBB score compared to the PHIEF-Cell group (6.2 ± 2.6) and THI hydrogel group (5.7 ± 1.5) (Fig. 7a1). Notably, 50% of the experimental rats received a BBB point being equal to or larger than 7 on day 28 post-surgery, and 66.7% on day 56 in the THIEF-Cell group. By contrast, no animal had received ≥7 points on either day 28 or day 56 post-surgery in the SCI group. It has to emphasize that half of the rats received ≥7 points in the THI hydrogel and PHIEF-Cell group on day 56 post-surgery too (Fig. 7a2). According to the definition and criteria of BBB scale, a 7 score represents that those three joints of the hind limb are all able to conduct extensive movement, while an 8 or more score represents plantar support of the paw. Herein, treatment with the THIEF-cell group exhibited its better therapeutic effect in locomotor recovery of the hind limbs in comparison to the other groups.

H&E staining was applied 7 days and 56 days post-surgery to assess the tissue cavity and nerve fiber at both the Rostral and Caudal areas (Fig. 5c and Fig. S11). Great loss of nerve fibers was found in the SCI group, which were greatly reduced in the THIEF-Cell, THI hydrogel group and PHIEF-Cell groups. Besides, the neural fibers at the Rostral and Caudal areas were more structured and oriented in both the THI hydrogel and the THIEF-Cell groups at both day 7 and day 56, indicating a better preservation of the original nerve fiber tissue. The immunofluorescent staining of spinal cord sagittal sections was further performed to investigate the anatomical basis of the motor function restoration and neurogenesis. The neurofilaments (NF200), a specific marker of mature neurons that is negatively correlated with the GFAP, was selected to indicate the axon regeneration at the lesion site. The tissues were analyzed throughout both the lesion and adjacent regions and the rostral and caudal distant segments of injured spinal cord (Fig. 7b), showing the significant regenerative effect of the THIEF-Cell group. The density of NF200 positive areas in all the lesion site and rostral and caudal areas exhibited an obvious superiority in the THIEF-Cell group compared to the SCI group. The mean percentages of the $NF200^{+}$ area and the $GFAP^{+}$ area of the excessive representative

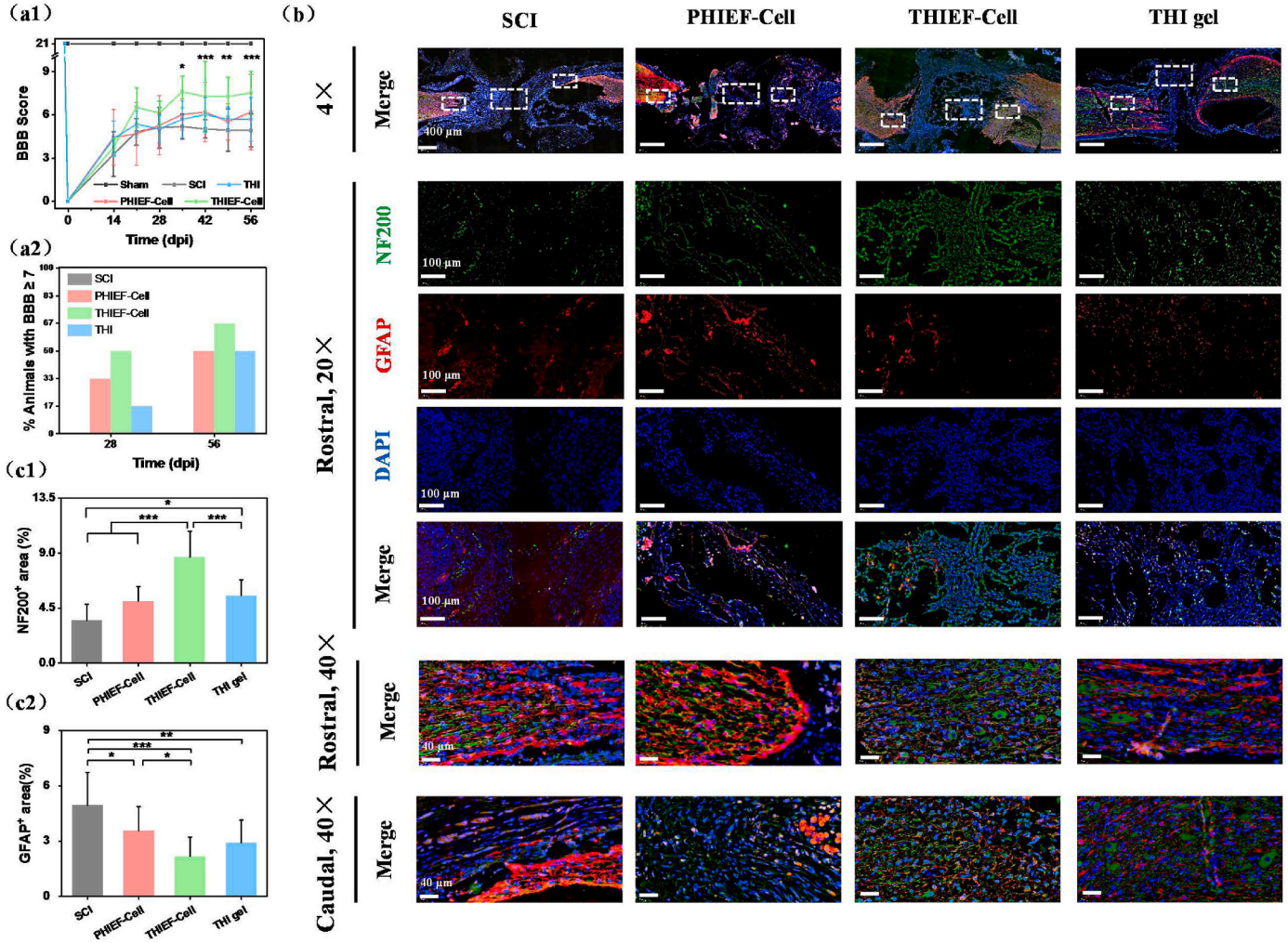


**Fig. 7.** Assessment of motor functional recovery and axon regeneration of spinal cord transected rats after treatment by BMSC-encapsulated hydrogels at 56 days post surgery. (a1) Functional recovery evaluated through Basso-Beattie-Bresnahan (BBB) score. (a2) Analysis of % of animals with a BBB score ≥7 on day 28 and 56 post surgery, suggesting the function restoration in the presence of BMSCs–containing ROS responsive hydrogel. (b) NF200 (neurofilament-200, marker of axon) and GFAP double immunofluorescence staining of nerve fibers and glial scars. The magnified images show the specific areas in the white boxes, and nerve structure in rostral and caudal regions. Quantitative analysis of (c1) NF200 positive and (c2) GFAP positive areas, showing a better neuron preservation and axon regeneration effect of BMSCs-encapsulated ROS-scavenging hydrogel. (d) Tuj-1 (tubulin-III, marker of neurogenesis) and MAP-2 (microtubule-associated protein-2, marker of mature neurons) immunofluorescence double staining images of nerve structure. (e) The magnified images show specific areas in the white boxes. The dashed lines outline the 2 mm transection. $^{*}p < 0.05$, $^{**}p < 0.01$, $^{***}p < 0.001$.

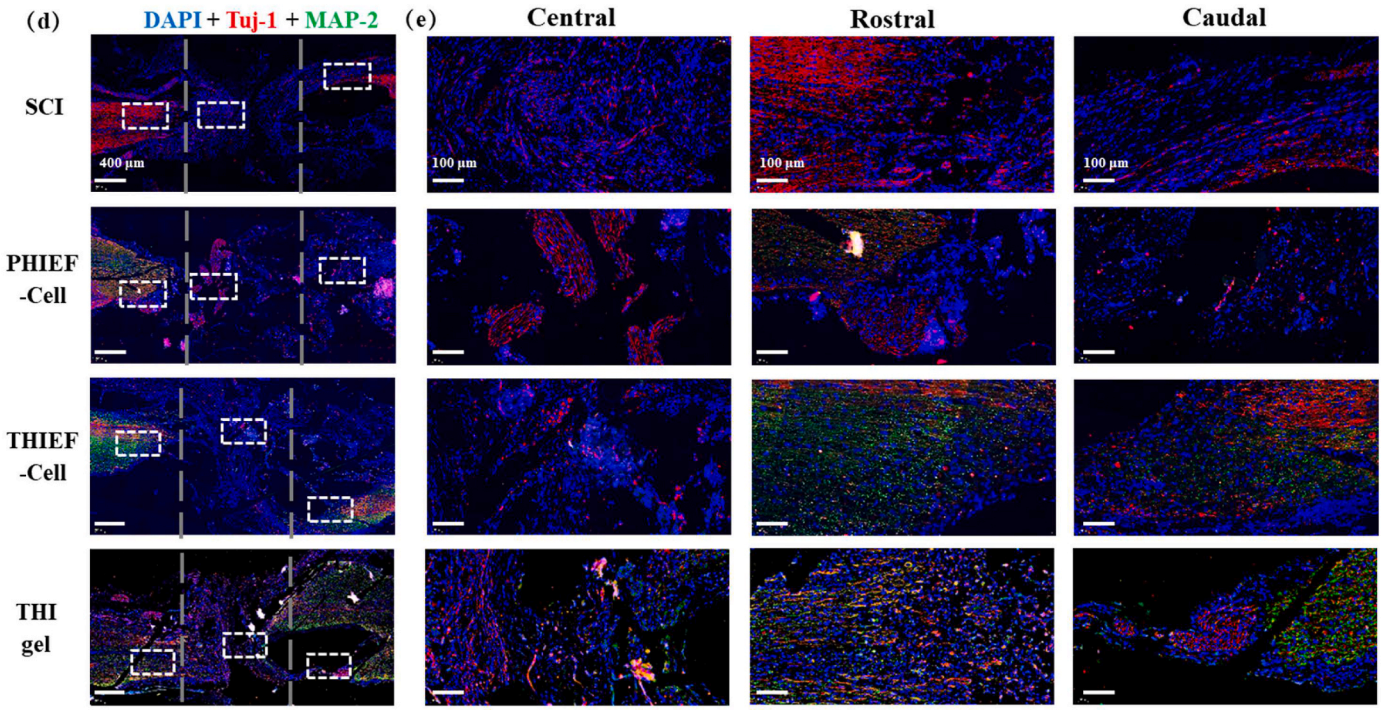


**Fig. 7.** (*continued*).

micrographs were calculated by Image J. Fig. 7c1 shows that the mean $NF200^+$ area of the THIEF-Cell group (8.7 ± 2.1%) was significantly larger than those of other groups ($p < 0.001$). The $NF200^+$ area in the THI hydrogel group was also significantly larger than that of the SCI group ($p < 0.05$). Comprehensively, the ROS-scavenging hydrogel modulates the hostile oxidative microenvironment, and thus ensures the enhanced endogenous axon regeneration. The encapsulated BMSCs within the ROS-scavenging hydrogel also provide the promotion in axon regeneration. More importantly, no significant difference was found between the PHIEF-Cell group and the SCI group with respect to axon regeneration. Therefore, the protection of the encapsulated BMSCs in the oxidative microenvironment is vital and indispensable, so that the promotion efficacy of BMSCs can be maximized in axon regeneration. These results are in good agreement with previous results on promoting axon regeneration via the elimination of oxidative stress by CONPs [27] and SeNPs [28].

It is widely believed that the endogenous neural stem and/or neural progenitor cells can home towards the lesion site and differentiate into specific cell lineage both *in vitro* and *in vivo* under certain circumstance after SCI occurrence, although a majority of which become astrocytes at last [90–92]. Therefore, a quantitative analysis of the $GFAP^+$ area was conducted. Fig. 7c2 shows that the THIEF-Cell group exhibited the least $GFAP^+$ area (2.2 ± 1.0%) and thus a smaller number of reactive astrocytes, which was significantly smaller than those of the PHIEF-Cell (3.6 ± 1.3%, $p < 0.05$) and SCI groups (4.9 ± 1.8, $p < 0.001$). Besides, the THI hydrogel group (2.9 ± 1.2%) also exhibited a significant smaller value compared to the SCI group ($p < 0.01$). Intriguingly, the PHIEF-Cell exhibited a significant difference compared to the SCI group too ($p < 0.05$), which is likely attributed to its good biocompatibility. The density and distribution of NF200 are negatively correlated with the GFAP, suggesting the nerve tissue regeneration to some extent instead of glial scar expansion [21].

Apart from the axon regeneration, the neurogenesis behavior was also investigated. The immunofluorescence staining of the Tuj-1 and microtubule-associated protein-2 (MAP-2) was used to identify the neuron at the early stage and the neuron dendrites, respectively. Fig. 7d shows that the THIEF-Cell group exhibited more $MAP\text{-}2^+$ area in the rostral and caudal areas compared to the SCI and PHIEF-Cell groups. However, in the central site the intensity of $MAP\text{-}2^+$ and $Tuj\text{-}1^+$ was almost same among all the groups.

Additionally, the CD31 and alpha smooth muscle actin (α-SMA) labeling was used to characterize the angiogenesis in the lesion sites of the transected spinal cords tissue on day 56 post-surgery (Fig. S12). Only a slight promotion of the angiogenesis without significance was observed in the THIEF-Cell group.

Although it has been widely believed that the resilience of the CNS is notable, the ability to regenerate axons is lacking, and the inherent regenerative capacity is largely lost during neuronal maturation [93]. Thus, the self-healing and endogenous axon regeneration depends largely on the neural differentiation of the endogenous neural stem cells that home and migrate to the lesion site. Briefly, the differentiated neurons could integrate with the residual neurons to reconstruct the neurite and synapse so that the nerve excitation signal could be well conducted and transmitted, resulting in the behavior restoration. Therefore, the neurogenesis and axon sprouting become vital. ROS can exhibit different effects on the neurogenesis and axon regeneration according to their concentration and types [94]. Without timely scavenging, the excessive ROS produced by the activated microglia and macrophage in the lesion site would degenerate the axon before kill the neuron or neural stem cells [95], prohibiting the axon regeneration. The self-renewal and differentiation phases of NPCs are also regulated by ROS. For example, a proper concentration of ROS increases neurite outgrowth in the neurocytes, such as the PC12 cells, hippocampal cells, neural stem cells and primary neuron cells [96,97]. It seems that only the non-neural cells-produced ROS (especially the immune cells-produced ROS) in a high concentration would reduce the tissue preservation and meanwhile prohibit the neurogenesis and lead to the regeneration failure, whereas the controlled production of ROS is essential for normal nervous system development. Thus, our ROS-scavenging hydrogels can eliminate the overproduced ROS in the microenvironment to attenuate excessive inflammation. On this account, massive neuron cells and nerve tissue can be well preserved during the secondary inflammation process. Considering the similar anti-inflammation efficacy of the THIEF-cell and THI groups, some of the

enhanced NF200+ nerve fibers in the THIEF-cell group are indicative of the endogenous neurogenesis.

Transplantation of MSCs in the lesion site post SCI is effective to enhance the preservation of original axons [98], and exhibit higher BBB scores compared with that of spinal progenitor cells [75]. In this study, we found that the BMSCs could enhance the axon regeneration and motor restoration in the ROS-scavenging hydrogel, whereas show no effect in the non ROS-responsive hydrogel. This would imply that the niche of the transplanted BMSCs takes a decisive role with respect to maintenance of their functions and promotion of neural regeneration. The exact roles of the transplanted stem cells still remain in dispute. Damaged cell replacement, immuno-regulation and paracrine effect are the three acknowledged functions to explain the stem cell-based axon regeneration. RNA sequencing of transplanted BMSCs in a SCI model shows an upregulated expression of Tuj-1 and GFAP, suggesting the possibility of neuron-like cell and astrocyte differentiation [99]. However, the MSCs are differentiated into a large number of oligodendrocytes (54.5 ± 9.1%) and astrocytes (22.1 ± 7.6%) with only a few of neurons (3.7 ± 0.9%). For massive neuron differentiation, the overexpression of NT-3 and TrkC [100], or a pre-induced differentiation *in vitro* via NT-3 and retinoic acid [101] are required. So far, the paracrine effect theory has gained more recognition, i.e. the stem cells secret various cytokines such as bFGF, ciliary neurotrophic factor (CNTF), nerve growth factor (NGF), glial cell line derived neurotrophic factor (GDNF) and vascular endothelial growth factor (VEGF) etc. in the SCI site [75,102]. Although the exact roles of the transplanted BMSCs are not the focus of current study, they deserve further investigation in the future. For further investigation, techniques such as RNA-sequencing and/or even the single-cell sequencing would be helpful to identify the exact signal pathways and the critical molecular mechanism.

Nonetheless, compared to the previously reported results on stem cell-encapsulated hydrogels for SCI treatment [20,103], our BMSCs-encapsulated ROS-scavenging hydrogel (THIEF-Cells group) significantly reduced the expression of inflammatory cytokines due to the ROS-responsive thioketal component and thus the protection of BMSCs from oxidative stress. It is known that severe inflammation mostly takes place in the first 7 days post-injury. When the proinflammatory process persists, the pro-regenerative process will be inhibited [104,105], resulting in the axon degradation and excessive formation of fibrotic scar and glial scar. Meanwhile, less nerve tissue will be preserved, inhibiting the regeneration process and aggravating the difficulties of motor recovery. On the contrary, it is beneficial to reduce inflammation and accelerate the repair process by reducing the infiltration of inflammatory cells or by inducing the polarization to M2 phenotype at the earlier stage post surgery [106,107], so that the transplanted stem cells are able to promote regeneration, and the scar formation would be alleviated. The therapeutic efficacy at day 7 post-surgery *in vivo* showed a better nerve fiber preservation and attenuated fibrotic scar formation. The long-term experiments did reveal the promotion of behavior restoration of ROS-scavenging hydrogel and BMSCs, as confirmed by the BBB scores and the quantitative analysis of the $NF200^{+}$ area.

There are still large rooms to optimize our materials system [108]. First, without a specific design of the patterning or oriented macro-porous structure, our hydrogel seems helpless in the directional guidance of the regenerated axons, which somehow present random in the lesion site. Second, the degradation process of the THIEF-Cells or the THI hydrogel group should be modulated to better match with the axon sprouting and regeneration processes. Third, the exact mechanisms of THIEF-Cell group on promoting the nerve repair and regeneration remain unclear at a molecular biology level. Finally, multiple target-responsive biomaterials with combined functions and specific spatial structure may better guide oriented regrowth of the regenerated axons and achieve better functional recovery.

## 4. Conclusion

A BMSC-encapsulated ROS-scavenging hydrogel was fabricated by one-pot synthesis of thioketal-containing hyperbranched polymer (HBPAK), biocompatible HA-MA and IKVAV peptides encapsulated with cell growth factors and BMSCs. Such a hydrogel was of high biocompatibility and could significantly attenuate the oxidative microenvironment *in vitro* and *in vivo*. Application of the BMSCs-encapsulated ROS-scavenging hydrogel to the lesion site in a rat spinal cord transection model, significantly alleviated the oxidation, inflammation and cell apoptosis, resulting in better neurogenesis and motor recovery accompanied with attenuation of scar formation *in vivo*. By contrast, transplantation of BMSCs in non ROS-responsive hydrogel showed an overall comparable performance to the SCI control, which was poorer than the ROS-scavenging hydrogel alone. Therefore, the use of our ROS-scavenging hydrogel represents a promising strategy for stem-cell-based therapies of CNS diseases via the comprehensive regulation of the hostile pathological microenvironment.

## Ethics approval

The animal experiment operations were approved by the Experimental Animal Ethics Committee of Hangzhou Medical College (Application Number: 200020015).

## CRediT authorship contribution statement

**Ziming Li:** Conceptualization, Investigation, Data curation, Methodology, Visualization, Writing – original draft, revision & editing. **Tengfei Zhao:** Investigation, Methodology, Visualization. **Jie Ding:** Investigation. **Haochen Gu:** Investigation, Methodology. **Qiaoxuan Wang:** Methodology. **Yifan Wang:** Methodology. **Deteng Zhang:** Conceptualization, Resources, Methodology. **Changyou Gao:** Conceptualization, Discussion, Supervision, Methodology, Resources, Funding acquisition, Writing – review & editing.

## Declaration of competing interest

The authors declare that they have no known competing financial interests or personal relationships that could have appeared to influence the work reported in this paper.

## Acknowledgment

This study is financially supported by the Natural Science Foundation of Zhejiang Province (LD21E030001) and National Natural Science Foundation of China (51873188).

## Appendix A. Supplementary data

Supplementary data to this article can be found online at https://doi.org/10.1016/j.bioactmat.2022.04.029.

## References

[1] H. Cowan, C. Lakra, M. Desai, Autonomic dysreflexia in spinal cord injury, BMJ Br. Med. J. (Clin. Res. Ed.) 371 (2020) m3596.
[2] W. Jiang, M. Li, F. He, L. Zhu, Inhibition of NLRP3 inflammasome attenuates spinal cord injury-induced lung injury in mice, J. Cell. Physiol. 234 (5) (2019) 6012–6022.
[3] S.L. James, A. Theadom, R.G. Ellenbogen, M.S. Bannick, W. Montjoy-Venning, L. R. Lucchesi, N. Abbasi, R. Abdulkader, H.N. Abraha, J.C. Adsuar, M. Afarideh, S. Agrawal, et al., Global, regional, and national burden of traumatic brain injury and spinal cord injury, 1990–2016: a systematic analysis for the Global Burden of Disease Study 2016, Lancet Neurol. 18 (1) (2019) 56–87.
[4] T.H. Hutson, S. Di Giovanni, The translational landscape in spinal cord injury: focus on neuroplasticity and regeneration, Nat. Rev. Neurol. 15 (12) (2019) 732–745.

[5] J.H. Badhiwala, J.R. Wilson, C.D. Witiw, J.S. Harrop, A.R. Vaccaro, B. Aarabi, R. G. Grossman, F.H. Geisler, M.G. Fehlings, The influence of timing of surgical decompression for acute spinal cord injury: a pooled analysis of individual patient data, Lancet Neurol. 20 (2) (2021) 117–126.
[6] M.E. Schwab, D. Bartholdi, Degeneration and regeneration of axons in the lesioned spinal cord, Physiol. Rev. 76 (2) (1996) 319–370.
[7] P. Pacher, J.S. Beckman, L. Liaudet, Nitric oxide and peroxynitrite in health and disease, Physiol. Rev. 87 (1) (2007) 315–424.
[8] Y. Wen, S. Yu, Y. Wu, R. Ju, H. Wang, Y. Liu, Y. Wang, Q. Xu, Spinal cord injury repair by implantation of structured hyaluronic acid scaffold with PLGA microspheres in the rat, Cell Tissue Res. 364 (1) (2016) 17–28.
[9] T.-F. Zhao, Y.-B. Jing, X.-P. Zhou, J.-K. Wang, X.-P. Huang, L.-S. Gao, Y.-J. Zhu, L.-J. Wang, Z.-R. Gou, C.-Z. Liang, K. Xu, F.-C. Li, et al., PHBV/PLA/Col-based nanofibrous scaffolds Promote recovery of locomotor function by decreasing reactive astrogliosis in a hemisection spinal cord injury rat model, J. Biomed. Nanotechnol. 14 (11) (2018) 1921–1933.
[10] B. Kaplan, U. Merdler, A.A. Szklanny, I. Redenski, S. Guo, Z. Bar-Mucha, N. Michael, S. Levenberg, Rapid prototyping fabrication of soft and oriented polyester scaffolds for axonal guidance, Biomaterials 251 (2020) 120062.
[11] C.M. Dumont, M.A. Carlson, M.K. Munsell, A.J. Ciciriello, K. Strnadova, J. Park, B.J. Cummings, A.J. Anderson, L.D. Shea, Aligned hydrogel tubes guide regeneration following spinal cord injury, Acta Biomater. 86 (2019) 312–322.
[12] J. Park, Y. Zhang, E. Saito, S.J. Gurczynski, B.B. Moore, B.J. Cummings, A. J. Anderson, L.D. Shea, Intravascular innate immune cells reprogrammed via intravenous nanoparticles to promote functional recovery after spinal cord injury, Proc. Natl. Acad. Sci. U. S. A. 116 (30) (2019) 14947–14954.
[13] R. Zhu, X. Zhu, Y. Zhu, Z. Wang, X. He, Z. Wu, L. Xue, W. Fan, R. Huang, Z. Xu, X. Qi, W. Xu, et al., Immunomodulatory layered double hydroxide nanoparticles enable neurogenesis by targeting transforming growth factor-beta receptor 2, ACS Nano 15 (2) (2021) 2812–2830.
[14] X.-J. Du, Y.-X. Chen, Z.-C. Zheng, N. Wang, X.-Y. Wang, F.-E. Kong, Neural stem cell transplantation inhibits glial cell proliferation and P2X receptor-mediated neuropathic pain in spinal cord injury rats, Neural Regen. Res. 14 (5) (2019) 876–885.
[15] M. Takano, S. Kawabata, S. Shibata, A. Yasuda, S. Nori, O. Tsuji, N. Nagoshi, A. Iwanami, H. Ebise, K. Horiuchi, H. Okano, M. Nakamura, Enhanced functional recovery from spinal cord injury in aged mice after stem cell transplantation through HGF induction, Stem Cell Rep. 8 (3) (2017) 509–518.
[16] X. Li, C. Zhang, A.E. Haggerty, J. Yan, M. Lan, M. Seu, M. Yang, M.M. Marlow, I. Maldonado-Lasunción, B. Cho, Z. Zhou, L. Chen, et al., The effect of a nanofiber-hydrogel composite on neural tissue repair and regeneration in the contused spinal cord, Biomaterials 245 (2020) 119978.
[17] L.T.A. Hong, Y.M. Kim, H.H. Park, D.H. Hwang, Y. Cui, E.M. Lee, S. Yahn, J. K. Lee, S.C. Song, B.G. Kim, An injectable hydrogel enhances tissue repair after spinal cord injury by promoting extracellular matrix remodeling, Nat. Commun. 8 (1) (2017) 533.
[18] J. Chedly, S. Soares, A. Montembault, Y. von Boxberg, M. Veron-Ravaille, C. Mouffle, M.-N. Benassy, J. Taxi, L. David, F. Nothias, Physical chitosan microhydrogels as scaffolds for spinal cord injury restoration and axon regeneration, Biomaterials 138 (2017) 91–107.
[19] L.-M. Li, M. Han, X.-C. Jiang, X.-Z. Yin, F. Chen, T.-Y. Zhang, H. Ren, J.-W. Zhang, T.-J. Hou, Z. Chen, H.-W. Ou-Yang, Y. Tabata, et al., Peptide-tethered hydrogel scaffold promotes recovery from spinal cord transection via synergism with mesenchymal stem cells, ACS Appl. Mater. Interfaces 9 (4) (2017) 3330–3342.
[20] M. Boido, M. Ghibaudi, P. Gentile, E. Favaro, R. Fusaro, C. Tonda-Turo, Chitosan-based hydrogel to support the paracrine activity of mesenchymal stem cells in spinal cord injury treatment, Sci. Rep. 9 (1) (2019) 6402.
[21] L. Li, B. Xiao, J. Mu, Y. Zhang, C. Zhang, H. Cao, R. Chen, H.K. Patra, B. Yang, S. Feng, Y. Tabata, N.K.H. Slater, et al., A MnO2 nanoparticle-dotted hydrogel promotes spinal cord repair via regulating reactive oxygen species microenvironment and synergizing with mesenchymal stem cells, ACS Nano 13 (12) (2019) 14283–14293.
[22] W. Xu, L. Chi, R. Xu, Y. Ke, C. Luo, J. Cai, M. Qiu, D. Gozal, R. Liu, Increased production of reactive oxygen species contributes to motor neuron death in a compression mouse model of spinal cord injury, Spinal Cord 43 (4) (2005) 204–213.
[23] Z. Liu, X. Yao, W. Jiang, W. Li, S. Zhu, C. Liao, L. Zou, R. Ding, J. Chen, Advanced oxidation protein products induce microglia-mediated neuroinflammation via MAPKs-NF-κB signaling pathway and pyroptosis after secondary spinal cord injury, J. Neuroinflammation 17 (1) (2020) 90.
[24] X. Li, J. Zhan, Y. Hou, Y. Hou, S. Chen, D. Luo, J. Luan, L. Wang, D. Lin, Coenzyme Q10 regulation of apoptosis and oxidative stress in H2O2 induced BMSC death by modulating the Nrf-2/NQO-1 signaling pathway and its application in a model of spinal cord injury, Oxid. Med. Cell. Longev. 2019 (2019) 6493081.
[25] H.N. Bhagavan, R.K. Chopra, Coenzyme Q10: absorption, tissue uptake, metabolism and pharmacokinetics, Free Radic 40 (5) (2006) 445–453.
[26] N.S. Pegoraro, J. Mattiazzi, E.F. da Silveira, J.H. Azambuja, E. Braganhol, L. Cruz, Improved photostability and cytotoxic effect of coenzyme Q10 by its association with vitamin E acetate in polymeric nanocapsules, Pharmaceut. Dev. Technol. 23 (4) (2018) 400–406.
[27] J.-W. Kim, C. Mahapatra, J.-Y. Hong, M.S. Kim, K.W. Leong, H.-W. Kim, J. K. Hyun, Functional recovery of contused spinal cord in rat with the injection of optimal-dosed cerium oxide nanoparticles, Adv. Sci. 4 (10) (2017) 1700034.
[28] W. Wang, X. Huang, Y. Zhang, G. Deng, X. Liu, C. Fan, Y. Xi, J. Yu, X. Ye, Se@SiO2 nanocomposites suppress microglia-mediated reactive oxygen species during spinal cord injury in rats, RSC Adv. 8 (29) (2018) 16126–16138.
[29] A. Pal, A. Singh, T.C. Nag, P. Chattopadhyay, R. Mathur, S. Jain, Iron oxide nanoparticles and magnetic field exposure promote functional recovery by attenuating free radical-induced damage in rats with spinal cord transection, Int. J. Nanomed. 8 (2013) 2259–2272.
[30] J.E. Hachmeister, L. Valluru, F. Bao, D. Liu, Mn (III) tetrakis (4-benzoic acid) porphyrin administered into the intrathecal space reduces oxidative damage and neuron death after spinal cord injury: a comparison with methylprednisolone, J. Neurotrauma 23 (12) (2006) 1766–1778.
[31] Y. Zhang, L. Li, J. Mu, J. Chen, S. Feng, J. Gao, Implantation of a functional TEMPO-hydrogel induces recovery from rat spinal cord transection through promoting nerve regeneration and protecting bladder tissue, Biomater. Sci. 8 (6) (2020) 1695–1701.
[32] T.-H. Zhang, F. Lin, W.-G. Liu, Y.-X. Liu, Z.-H. Guo, C.-S. Xiao, X.-L. Zhuang, X.-S. Chen, Reactive oxide species-scavenging lipid-polymer nanoparticles for neuroprotection after spinal cord injury, Appl. Mater. Today 24 (2021) 101109.
[33] J. Ding, Y. Yao, J. Li, Y. Duan, J.R. Nakkala, X. Feng, W. Cao, Y. Wang, L. Hong, L. Shen, Z. Mao, Y. Zhu, et al., A reactive oxygen species scavenging and O2 generating injectable hydrogel for myocardial infarction treatment in vivo, Small 16 (48) (2020) 2005038.
[34] Y. Yao, J. Ding, Z. Wang, H. Zhang, J. Xie, Y. Wang, L. Hong, Z. Mao, J. Gao, C. Gao, ROS-responsive polyurethane fibrous patches loaded with methylprednisolone (MP) for restoring structures and functions of infarcted myocardium in vivo, Biomaterials 232 (2020) 119726.
[35] Z. Yan, W. Bing, C. Ding, K. Dong, J. Ren, X. Qu, A H2O2-free depot for treating bacterial infection: localized cascade reactions to eradicate biofilms in vivo, Nanoscale 10 (37) (2018) 17656–17662.
[36] V.B. Jovanović, A.Z. Penezić-Romanjuk, I.D. Pavićević, J.M. Aćimović, L. M. Mandić, Improving the reliability of human serum albumin-thiol group determination, Anal. Biochem. 439 (1) (2013) 17–22.
[37] Q. Ge, X. Wang, Y. Luo, X. Zheng, L. Ma, E7-modified substrates to promote adhesion and maintain stemness of mesenchymal stem cells, Macromol. Biosci. 21 (4) (2021) 2000384.
[38] D. Zhang, Y. Yao, Y. Duan, X. Yu, H. Shi, J.R. Nakkala, X. Zuo, L. Hong, Z. Mao, C. Gao, Surface-anchored graphene oxide nanosheets on cell-scale micropatterned poly(d,l-lactide-co-caprolactone) conduits promote peripheral nerve regeneration, ACS Appl. Mater. Interfaces 12 (7) (2020) 7915–7930.
[39] H. Niu, X. Li, H. Li, Z. Fan, J. Ma, J. Guan, Thermosensitive, fast gelling, photoluminescent, highly flexible, and degradable hydrogels for stem cell delivery, Acta Biomater. 83 (2019) 96–108.
[40] J. Lam, W.E. Lowry, S.T. Carmichael, T. Segura, Delivery of iPS-NPCs to the stroke cavity within a hyaluronic acid matrix promotes the differentiation of transplanted cells, Adv. Funct. Mater. 24 (44) (2014) 7053–7062.
[41] Y. Wang, Bioadaptability: an innovative concept for biomaterials, J. Mater. Sci. Technol. 32 (9) (2016) 801–809.
[42] A. Banerjee, M. Arha, S. Choudhary, R.S. Ashton, S.R. Bhatia, D.V. Schaffer, R. S. Kane, The influence of hydrogel modulus on the proliferation and differentiation of encapsulated neural stem cells, Biomaterials 30 (27) (2009) 4695–4699.
[43] W. Sun, T. Incitti, C. Migliaresi, A. Quattrone, S. Casarosa, A. Motta, Viability and neuronal differentiation of neural stem cells encapsulated in silk fibroin hydrogel functionalized with an IKVAV peptide, Tissue Eng. Regen. Med. 11 (5) (2017) 1532–1541.
[44] Y. Yao, H. Zhang, Z. Wang, J. Ding, S. Wang, B. Huang, S. Ke, C. Gao, Reactive oxygen species (ROS)-responsive biomaterials mediate tissue microenvironments and tissue regeneration, J. Mater. Chem. B 7 (33) (2019) 5019–5037.
[45] C.M. Madl, B.L. LeSavage, R.E. Dewi, K.J. Lampe, S.C. Heilshorn, Matrix remodeling enhances the differentiation capacity of neural progenitor cells in 3D hydrogels, Adv. Sci. 6 (4) (2019) 1801716.
[46] C.M. Madl, B.L. LeSavage, R.E. Dewi, C.B. Dinh, R.S. Stowers, M. Khariton, K. J. Lampe, D. Nguyen, O. Chaudhuri, A. Enejder, S.C. Heilshorn, Maintenance of neural progenitor cell stemness in 3D hydrogels requires matrix remodelling, Nat. Mater. 16 (12) (2017) 1233–1242.
[47] L. Šoltés, R. Mendichi, G. Kogan, J. Schiller, M. Stankovská, J. Arnhold, Degradative action of reactive oxygen species on hyaluronan, Biomacromolecules 7 (3) (2006) 659–668.
[48] S.-J. Yu, H.-J. Kim, E.S. Lee, C.-G. Park, S.J. Cho, S.-H. Jeon, β-catenin accumulation is associated with increased expression of nanog protein and predicts maintenance of MSC self-renewal, Cell Transplant. 26 (2) (2017) 365–377.
[49] A.A. Khan, T.J. Huat, A. Al Mutery, A.T. El-Serafi, H.H. Kacem, S.H. Abdallah, M. F. Reza, J.M. Abdullah, H. Jaafar, Significant transcriptomic changes are associated with differentiation of bone marrow-derived mesenchymal stem cells into neural progenitor-like cells in the presence of bFGF and EGF, Cell Biosci. 10 (1) (2020) 126.
[50] M.C. Jimenez Hamann, C.H. Tator, M.S. Shoichet, Injectable intrathecal delivery system for localized administration of EGF and FGF-2 to the injured rat spinal cord, Exp. Neurol. 194 (1) (2005) 106–119.
[51] P. Wang, H. Wang, K. Ma, S. Wang, C. Yang, N. Mu, F. Yang, H. Feng, T. Chen, Novel cytokine-loaded PCL-PEG scaffold composites for spinal cord injury repair, RSC Adv. 10 (11) (2020) 6306–6314.
[52] H. Wu, Y. Wang, Y. Zhang, F. Xu, J. Chen, L. Duan, T. Zhang, J. Wang, F. Zhang, Breaking the vicious loop between inflammation, oxidative stress and

coagulation, a novel anti-thrombus insight of nattokinase by inhibiting LPS-induced inflammation and oxidative stress, Redox Biol. 32 (2020) 101500.
[53] F. da Costa Gonçalves, M. Grings, N.S. Nunes, F.O. Pinto, T.N.A. Garcez, F. Visioli, G. Leipnitz, A.H. Paz, Antioxidant properties of mesenchymal stem cells against oxidative stress in a murine model of colitis, Biotechnol. Lett. 39 (4) (2017) 613–622.
[54] K. Kemp, E. Mallam, K. Hares, J. Witherick, N. Scolding, A. Wilkins, Mesenchymal stem cells restore frataxin expression and increase hydrogen peroxide scavenging enzymes in Friedreich ataxia fibroblasts, PLoS One 6 (10) (2011) e26098-e26098.
[55] N. An, J. Yang, H. Wang, S. Sun, H. Wu, L. Li, M. Li, Mechanism of mesenchymal stem cells in spinal cord injury repair through macrophage polarization, Cell Biosci. 11 (1) (2021) 41.
[56] F. Liu, H. Qiu, M. Xue, S. Zhang, X. Zhang, J. Xu, J. Chen, Y. Yang, J. Xie, MSC-secreted TGF-β regulates lipopolysaccharide-stimulated macrophage M2-like polarization via the Akt/FoxO1 pathway, Stem Cell Res. Ther. 10 (1) (2019) 345.
[57] C. Li, G. Li, M. Liu, T. Zhou, H. Zhou, Paracrine effect of inflammatory cytokine-activated bone marrow mesenchymal stem cells and its role in osteoblast function, J. Biosci. Bioeng. 121 (2) (2016) 213–219.
[58] E. Redondo-Castro, C. Cunningham, J. Miller, L. Martuscelli, S. Aoulad-Ali, N. J. Rothwell, C.M. Kielty, S.M. Allan, E. Pinteaux, Interleukin-1 primes human mesenchymal stem cells towards an anti-inflammatory and pro-trophic phenotype in vitro, Stem Cell Res. Ther. 8 (1) (2017) 79.
[59] T. Gong, L. Liu, W. Jiang, R. Zhou, DAMP-sensing receptors in sterile inflammation and inflammatory diseases, Nat. Rev. Immunol. 20 (2) (2020) 95–112.
[60] Z. Liu, X. Yao, W. Jiang, W. Li, S. Zhu, C. Liao, L. Zou, R. Ding, J. Chen, Advanced oxidation protein products induce microglia-mediated neuroinflammation via MAPKs-NF-κB signaling pathway and pyroptosis after secondary spinal cord injury, J. Neuroinflammation 17 (1) (2020) 90.
[61] W. Wu, S. Wang, Q. Liu, X. Wang, T. Shan, Y. Wang, Cathelicidin-WA attenuates LPS-induced inflammation and redox imbalance through activation of AMPK signaling, Free Radic. Biol. Med. 129 (2018) 338–353.
[62] X. Zhengxing, H. Aiying, Z. Zongqiang, M. zengli, Carbon monoxide protects neural stem cells against iron overload by modulating the crosstalk between Nrf2 and NF-κB signaling, Neurochem. Res. 47 (5) (2022) 1383–1394.
[63] N.P. Visavadiya, S.P. Patel, J.L. VanRooyen, P.G. Sullivan, A.G. Rabchevsky, Cellular and subcellular oxidative stress parameters following severe spinal cord injury, Redox Biol. 8 (2016) 59–67.
[64] E.D. Hall, J.M. Bosken, Measurement of oxygen radicals and lipid peroxidation in neural tissues, Curr. Protoc. Neurosci. 48 (1) (2009) 7.17.1–7.17.51.
[65] S. Rao, Y. Lin, Y. Du, L. He, G. Huang, B. Chen, T. Chen, Designing multifunctionalized selenium nanoparticles to reverse oxidative stress-induced spinal cord injury by attenuating ROS overproduction and mitochondria dysfunction, J. Mater. Chem. B 7 (16) (2019) 2648–2656.
[66] Z. Li, Q. Wang, H. Hu, W. Zheng, C. Gao, Research advances of biomaterials-based microenvironment-regulation therapies for repair and regeneration of spinal cord injury, Biomed. Mater. 16 (5) (2021), 052002.
[67] L.M. Milich, C.B. Ryan, J.K. Lee, The origin, fate, and contribution of macrophages to spinal cord injury pathology, Acta Neuropathol. 137 (5) (2019) 785–797.
[68] L. Xu, B.O.A. Botchway, S. Zhang, J. Zhou, X. Liu, Inhibition of NF-κB signaling pathway by resveratrol improves spinal cord injury, Front. Neurosci. 12 (690) (2018).
[69] Z. Feng, L. Min, H. Chen, W. Deng, M. Tan, H. Liu, J. Hou, Iron overload in the motor cortex induces neuronal ferroptosis following spinal cord injury, Redox Biol. 43 (2021) 101984.
[70] B.A. McKenzie, V.M. Dixit, C. Power, Fiery cell death: pyroptosis in the central nervous system, Trends Neurosci. 43 (1) (2020) 55–73.
[71] W. Zhu, X. Chen, L. Ning, K. Jin, Network analysis reveals TNF as a major hub of reactive inflammation following spinal cord injury, Sci. Rep. 9 (1) (2019) 928.
[72] Y.O. Mukhamedshina, E.R. Akhmetzyanova, E.V. Martynova, S.F. Khaiboullina, L. R. Galieva, A.A. Rizvanov, Systemic and local cytokine profile following spinal cord injury in rats: a multiplex analysis, Front. Neurol. 8 (581) (2017).
[73] A. Sato, H. Ohtaki, T. Tsumuraya, D. Song, K. Ohara, M. Asano, Y. Iwakura, T. Atsumi, S. Shioda, Interleukin-1 participates in the classical and alternative activation of microglia/macrophages after spinal cord injury, J. Neuroinflammation 9 (1) (2012) 65.
[74] M. Nakamura, S. Okada, Y. Toyama, H. Okano, Role of IL-6 in spinal cord injury in a mouse model, Clin. Rev. Allergy Immunol. 28 (3) (2005) 197–203.
[75] J. Ruzicka, L. Machova-Urdzikova, J. Gillick, T. Amemori, N. Romanyuk, K. Karova, K. Zaviskova, J. Dubisova, S. Kubinova, R. Murali, E. Sykova, M. Jhanwar-Uniyal, et al., A comparative study of three different types of stem cells for treatment of rat spinal cord injury, Cell Transplant. 26 (4) (2017) 585–603.
[76] N.B. Pivovarova, S.B. Andrews, Calcium-dependent mitochondrial function and dysfunction in neurons, FEBS J. 277 (18) (2010) 3622–3636.
[77] R.R. Kotipatruni, V.R. Dasari, K.K. Veeravalli, D.H. Dinh, D. Fassett, J.S. Rao, p53-and Bax-mediated apoptosis in injured rat spinal cord, Neurochem. Res. 36 (11) (2011) 2063.
[78] J.E. Springer, R.D. Azbill, P.E. Knapp, Activation of the caspase-3 apoptotic cascade in traumatic spinal cord injury, Nat. Med. 5 (8) (1999) 943–946.
[79] A.P. Tran, P.M. Warren, J. Silver, The biology of regeneration failure and success after spinal cord injury, Physiol. Rev. 98 (2) (2018) 881–917.
[80] I.B. Wanner, M.A. Anderson, B. Song, J. Levine, A. Fernandez, Z. Gray-Thompson, Y. Ao, M.V. Sofroniew, Glial scar borders are formed by newly proliferated, elongated astrocytes that Interact to corral inflammatory and fibrotic cells via STAT3-dependent mechanisms after spinal cord injury, J. Neurosci. 33 (31) (2013) 12870–12886.
[81] J. Silva dos Santos, J.P. Gonçalves Cirino, P. de Oliveira Carvalho, M.M. Ortega, The pharmacological action of kaempferol in central nervous system diseases: a review, Front. Pharnacol. (2021).
[82] L. Yang, B.M. Conley, S.R. Cerqueira, T. Pongkulapa, S. Wang, J.K. Lee, K.-B. Lee, Effective modulation of CNS inhibitory microenvironment using bioinspired hybrid-nanoscaffold-based therapeutic interventions, Adv. Mater. 32 (43) (2020) 2002578.
[83] Y. Zhu, C. Soderblom, M. Trojanowsky, D.-H. Lee, J.K. Lee, Fibronectin matrix assembly after spinal cord injury, J. Neurotrauma 32 (15) (2014) 1158–1167.
[84] J.R. Nakkala, Z. Li, W. Ahmad, K. Wang, C. Gao, Immunomodulatory biomaterials and their application in therapies for chronic inflammation-related diseases, Acta Biomater. 123 (2021) 1–30.
[85] M.K. Gottipati, A.R. D'Amato, A.M. Ziemba, P.G. Popovich, R.J. Gilbert, TGFβ3 is neuroprotective and alleviates the neurotoxic response induced by aligned poly-l-lactic acid fibers on naïve and activated primary astrocytes, Acta Biomater. 117 (2020) 273–282.
[86] L. Yang, B.M. Conley, S.R. Cerqueira, T. Pongkulapa, S. Wang, J.K. Lee, K.-B. Lee, Effective modulation of CNS inhibitory microenvironment using bioinspired hybrid-nanoscaffold-based therapeutic interventions, Adv. Mater. 32 (43) (2020) 2002578.
[87] Y. Zhu, C. Soderblom, V. Krishnan, J. Ashbaugh, J.R. Bethea, J.K. Lee, Hematogenous macrophage depletion reduces the fibrotic scar and increases axonal growth after spinal cord injury, Neurobiol. Dis. 74 (2015) 114–125.
[88] C. Wang, Z. Gong, X. Huang, J. Wang, K. Xia, L. Ying, J. Shu, C. Yu, X. Zhou, F. Li, C. Liang, Q. Chen, An injectable heparin-Laponite hydrogel bridge FGF4 for spinal cord injury by stabilizing microtubule and improving mitochondrial function, Theranostics 9 (23) (2019) 7016–7032.
[89] C. Wang, M. Wang, K. Xia, J. Wang, F. Cheng, K. Shi, L. Ying, C. Yu, H. Xu, S. Xiao, C. Liang, F. Li, et al., A bioactive injectable self-healing anti-inflammatory hydrogel with ultralong extracellular vesicles release synergistically enhances motor functional recovery of spinal cord injury, Bioact. Mater. 6 (8) (2021) 2523–2534.
[90] F.H. Gage, Mammalian neural stem cells, Science 287 (5457) (2000) 1433–1438.
[91] K. Meletis, F. Barnabe-Heider, M. Carlen, E. Evergren, N. Tomilin, O. Shupliakov, J. Frisen, Spinal cord injury reveals multilineage differentiation of ependymal cells, PLoS Biol. 6 (7) (2008) e182.
[92] L.K. Hamilton, M.K. Truong, M.R. Bednarczyk, A. Aumont, K.J. Fernandes, Cellular organization of the central canal ependymal zone, a niche of latent neural stem cells in the adult mammalian spinal cord, Neuroscience 164 (3) (2009) 1044–1056.
[93] F. Bradke, S. Di Giovanni, J. Fawcett, Neuronal maturation:challenges and opportunities in a nascent field, Trends Neurosci. 43 (6) (2020) 360–362.
[94] A. Terzi, D.M. Suter, The role of NADPH oxidases in neuronal development, Free Radic. Biol. Med. 154 (2020) 33–47.
[95] K. Fukui, Reactive oxygen species induce neurite degeneration before induction of cell death, J. Clin. Biochem. Nutr. 59 (3) (2016) 155–159.
[96] X. Wang, Z. Wang, Y. Yao, J. Li, X. Zhang, C. Li, Y. Cheng, G. Ding, L. Liu, Z. Ding, Essential role of ERK activation in neurite outgrowth induced by α-lipoic acid, Biochim. Biophys. Acta Mol. Cell Res. 1813 (5) (2011) 827–838.
[97] M. Olguín-Albuerne, J. Morán, ROS produced by NOX2 controls in vitro development of cerebellar granule neurons development, ASN Neuro 7 (2) (2015), 1759091415578712.
[98] C. Yang, G. Wang, F. Ma, B. Yu, F. Chen, J. Yang, J. Feng, Q. Wang, Repeated injections of human umbilical cord blood-derived mesenchymal stem cells significantly promotes functional recovery in rabbits with spinal cord injury of two noncontinuous segments, Stem Cell Res. Ther. 9 (1) (2018) 136.
[99] R. Hakim, R. Covacu, V. Zachariadis, A. Frostell, S.R. Sankavaram, L. Brundin, M. Svensson, Mesenchymal stem cells transplanted into spinal cord injury adopt immune cell-like characteristics, Stem Cell Res. Ther. 10 (1) (2019) 115.
[100] X.-C. Qiu, H. Jin, R.-Y. Zhang, Y. Ding, X. Zeng, B.-Q. Lai, E.-A. Ling, J.-L. Wu, Y.-S. Zeng, Donor mesenchymal stem cell-derived neural-like cells transdifferentiate into myelin-forming cells and promote axon regeneration in rat spinal cord transection, Stem Cell Res. Ther. 6 (1) (2015) 105.
[101] K. Zhang, Z. Liu, G. Li, B.-Q. Lai, L.-N. Qin, Y. Ding, J.-W. Ruan, S.-X. Zhang, Y.-S. Zeng, Electro-acupuncture promotes the survival and differentiation of transplanted bone marrow mesenchymal stem cells pre-Induced with neurotrophin-3 and retinoic acid in gelatin sponge scaffold after rat spinal cord transection, Stem Cell Rev. 10 (4) (2014) 612–625.
[102] G.W.J. Hawryluk, A. Mothe, J. Wang, S. Wang, C. Tator, M.G. Fehlings, An in vivo characterization of trophic factor production following neural precursor cell or bone marrow stromal cell transplantation for spinal cord injury, Stem Cell. Dev. 21 (12) (2011) 2222–2238.
[103] A. Hejcl, J. Ruzicka, V. Proks, H. Mackova, S. Kubinova, D. Tukmachev, J. Cihlar, D. Horak, P. Jendelova, Dynamics of tissue ingrowth in SIKVAV-modified highly superporous PHEMA scaffolds with oriented pores after bridging a spinal cord transection, J. Mater. Sci. Mater. Med. 29 (7) (2018).
[104] B. Linnartz, Y. Wang, H. Neumann, Microglial immunoreceptor tyrosine-based activation and inhibition motif signaling in neuroinflammation, Int. J. Alzheimer's Dis. (2010).
[105] A. Kroner, Andrew D. Greenhalgh, Juan G. Zarruk, R. Passos dos Santos, M. Gaestel, S. David, TNF and increased intracellular iron alter macrophage polarization to a detrimental M1 phenotype in the injured spinal cord, Neuron 83 (5) (2014) 1098–1116.

[106] I. Francos-Quijorna, J. Amo-Aparicio, A. Martinez-Muriana, R. López-Vales, IL-4 drives microglia and macrophages toward a phenotype conducive for tissue repair and functional recovery after spinal cord injury, Glia 64 (12) (2016) 2079–2092.
[107] C. Wu, S. Chen, T. Zhou, K. Wu, Z. Qiao, Y. Zhang, N. Xin, X. Liu, D. Wei, J. Sun, H. Luo, L. Zhou, et al., Antioxidative and conductive nanoparticles-embedded cell niche for neural differentiation and spinal cord injury repair, ACS Appl. Mater. Interfaces 13 (44) (2021) 52346–52361.
[108] Wei-Hai Chen, Qi-Wei Chen, Qian Chen, Chunyan Cui, Shun Duan, Yongyuan Kang, Yang Liu, Yun Liu, Wali Muhammad, Shiqun Shao, Chengqiang Tang, Jinqiang Wang, Lei Wang, Meng-Hua Xiong, Lichen Yin, Kuo Zhang, Zhanzhan Zhang, Xu Zhen, Jun Feng, Changyou Gao, Zhen Gu, Chaoliang He, Jian Ji, Xiqun Jiang, Wenguang Liu, Zhuang Liu, Huisheng Peng, Youqing Shen, Linqi Shi, Xuemei Sun, Hao Wang, Jun Wang, Haihua Xiao, Fu-Jian Xu, Zhiyuan Zhong, Xian-Zheng Zhang, Xuesi Chen, Biomedical polymers: synthesis, properties, and applications, Science China Chemistry (2022), https://doi.org/10.1007/s11426-022-1243-5. In press.